

A THERMOMETRIC FILM SIMULATOR AND
AN APPLICATION TO THE FILM MOUNT OF
THE ARCASTONDE 1A SENSOR

Progress Report under
NASA Grant NGR 45-003-025

November 1967

University of Utah
Electrical Engineering Department

Forrest L. Staffanson
Shigetaka Kikkawa

Forrest L. Staffanson
Forrest L. Staffanson
Principal Investigator

ABSTRACT

A FORTRAN program is presented which uses the alternating direction implicit method of two-dimensional numerical integration for the calculation of the time-dependent temperature distribution over a planar thin plate having an arbitrary distribution of conductive, convective, and radioactive properties and boundary conditions. The program is applied to the film mount of the ARCAISONDE 1A meteorological rocketsonde temperature sensor. Observations are made relative to the film performance at 60 and 70 km altitude, particularly concerning conductive insulation from support posts, speed of response, susceptibility to radiation, and the heat conduction from attached thermistor and sonde wires.

TABLE OF CONTENTS

ABSTRACT	ii
LIST OF ILLUSTRATIONS AND TABLES	iv
I. INTRODUCTION	1
II. HEAT EQUATION	3
Characteristic Time Constant and Equilibrium Temperature . . .	9
III. TWO-DIMENSIONAL INTEGRATOR	11
Finite Difference Method	11
Explicit Method	11
Alternating Direction Implicit Method	14
IV. APPLICATION TO ARCASONDE 1A FILM	19
Film Configuration	19
Radiation Inputs	22
Convection Coefficients	26
Conductive Isolation	26
Time Constant	30
Radiation Error	36
Effect of Heat Conduction with the Wires	38
V. INTEGRATOR PROGRAM	42
GLOSSARY	52
BIBLIOGRAPHY	54

LIST OF ILLUSTRATIONS AND TABLES

<u>Figure</u>	<u>Page</u>
1.1 Typical planar thin substrate thermistor sensor	2
2.1 The physical two-dimensional system	5
2.2 Conductive coupling of adjacent volume elements	6
3.1 Two-dimensional grid	13
4.1 Arcasonde 1A film configuration and dimensions	20
4.2 Regions k of the film as seen from the "front" ($\ell = 1$) side .	21
4.3 Plots of local convection coefficient h_x (watt/m ² °K) and local recovery factor r_x versus distance x (cm) from leading edge for 256 m/sec at 70 km and 120 m/sec at 60 km	27
4.4 Steady-state temperature distribution at 60 km and 120 m/sec air speed in daytime shade	28
4.5 The difference between the steady-state temperature and the local characteristic equilibrium temperature ($T - T_e$) (60 km)	29
4.6 ($T - T_e$) insulated from support posts (60 km)	31
4.7 Steady-state temperature distribution at 70 km 256 m/sec air speed in daytime shade	32
4.8 The difference between the steady-state temperature and the local characteristic equilibrium temperature ($T - T_e$) (70 km)	33
4.9 ($T - T_e$) insulated from support post (70 km)	34
4.10 Transient temperature of junction at 60 and 70 km	36
4.11 The equilibrium temperature distribution of the film at 70 km under direct solar radiation	39
4.12 Temperature distribution with heat input at wire junctions .	41
5.1 Flow diagram	43

TABLES

<u>Table</u>	<u>Page</u>
4.1 Physical Properties Used For the Arcasonde 1A Film	21
4.2 Characteristic Time Constants (ρ cd/g seconds) at 70 km, of Junction, Silver (Outer Leg, near Junction), and Mylar (Remote from Silver and Frame), at Beginning ($t = 0$) and End ($t = 50$ sec) of transient. Also the Effective Time Constant of the Film at the Junction Respectively at 60 and 70 km, and at 70 km Without Solder	35
4.3 Wire Junction Temperatures when the Film is Under (a) Maximum Direct Solar Radiation (b) Sun-shaded Daytime Radiation, and (c) No Solar Illumination (Nighttime) Successive Differences are Parenthesized and Recovery and Atmospheric Temperatures are Included for Reference	37

I. INTRODUCTION

Films are gaining considerable attention as sensors for atmospheric thermometry in the mesosphere because of their inherent speed. The purpose of the present discussion is to describe a means of investigating the two-dimensional, time-varying temperature distribution in a film with a nonuniform pattern of thermal properties, boundaries, and sources, in a radiation environment with rarefied airflow.

Figure 1.1 illustrates a typical planar thin substrate type thermistor sensor. The thin film thermistor is deposited on a small area of the thin substrate and the substrate is supported by the frame. Electrical conduction to the thermistor film is made through electrically conductive thin film leads also deposited on the substrate.

The electrical resistance of the thermistor film varies according to temperature. Since the thermistor temperature is monitored by an electric current, ohmic heating occurs in the sensitive film. Some sensor designs use deposited regions of thermally conductive material near the thermistor film to dissipate this electric heat.

In addition to the analysis of future film-type sensors, this means of investigation is applicable to the film-mounted thermistor bead sensor in common use today. The film in these sensors presents a heat source or sink at the ends of the thermistor wires, depending on the thermal behavior of the film in the environment. The film in this case may include the solder or other materials constituting the wire-film junction. The heat flow between wire and film may be represented as a source or sink.

The computer program discussed below, hereafter called the "integrator," computes the time-varying two-dimensional temperature distribution $T(x,y,t)$ over the bounded plane of such films.

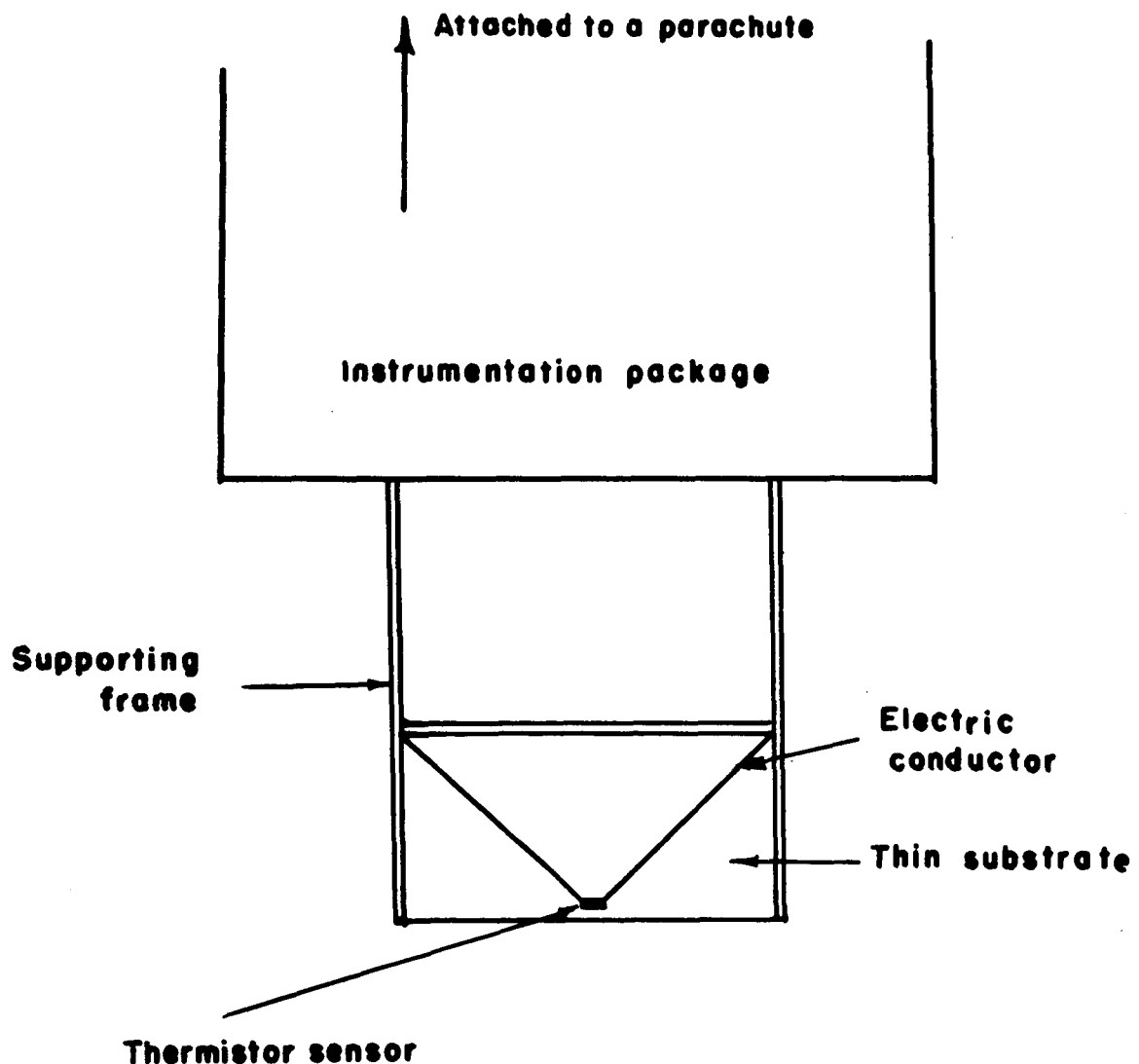


Fig. 1.1. Typical planar thin substrate thermistor sensor.

II. HEAT EQUATION

The flat plate under consideration is sufficiently thin that the temperature between its faces can be considered uniform. In this case, the heat input rate to a small volume element v is

$$(\rho cv)_{ij} \frac{\partial T}{\partial t} = (\text{conduction input})_{ij} + (\text{convection input})_{ij} \\ + (\text{radiation input})_{ij} + (\text{heat source input})_{ij}$$

where the subscripts i,j represent the position on the plate. The terms are expressed mathematically as follows:

$$(\text{conduction input})_{ij} = A \left[\frac{\partial}{\partial x} \left(kv \frac{\partial T}{\partial x} \right) \right]_{ij} + A \left[\frac{\partial}{\partial y} \left(kv \frac{\partial T}{\partial y} \right) \right]_{ij}$$

$$(\text{convection input})_{ij} = \left[hA (T_r - T_{ij}) \right]_{\text{front}} + \left[hA (T_r - T_{ij}) \right]_{\text{back}}$$

$$(\text{radiation input})_{ij} = \left[A q_r \right]_{\text{front}} + \left[A q_r \right]_{\text{back}}$$

$$- \left[\epsilon \sigma T_{ij}^4 \right]_{\text{front}} - \left[\epsilon \sigma T_{ij}^4 \right]_{\text{back}}$$

$$(\text{heat source input})_{ij} = q_{ij}$$

where

ρ = mass density of the plate
 c = specific heat of the plate
 T_{ij} = temperature of the plate
 T_r = recovery temperature
 h = convective coefficient
 q_r = radiative heat input
 ϵ = emissivity of the plate
 σ = Stefan-Boltzmann constant
 k = conductivity of the plate

An expression for the two-dimensional conductive heat transfer is derived as shown in Fig. 2.1. Consider small rectangular elements of the film. The net rate of heat increase of an element due to conduction is the algebraic sum of the conductive heat input from each of its neighboring elements. Referring to Fig. 2.1, this becomes for P_{ij} :

from $P_{i-1,j}$

$$\frac{2(kd)_{i-1,j} (kd)_{i,j} \Delta x}{(kd)_{i-1,j} + (kd)_{i,j}} \frac{T_{i-1,j} - T_{i,j}}{\Delta y}$$

from $P_{i+1,j}$

$$\frac{2(kd)_{i+1,j} (kd)_{i,j} \Delta x}{(kd)_{i+1,j} + (kd)_{i,j}} \frac{T_{i+1,j} - T_{i,j}}{\Delta y}$$

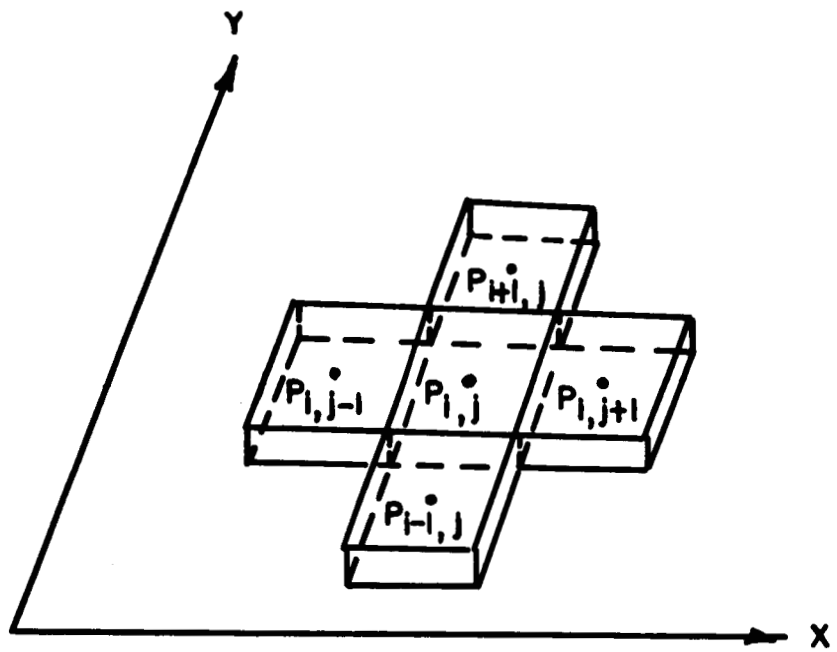


Fig. 2.1. The physical two-dimensional system.

from $p_{i,j-1}$

$$\frac{2(kd)_{i,j-1} (kd)_{i,j} \Delta y}{(kd)_{i,j-1} + (kd)_{i,j}} \frac{T_{i,j-1} - T_{i,j}}{\Delta x}$$

from $P_{i,j+1}$

$$\frac{2(kd)_{i,j+1} (kd)_{i,j} \Delta y}{(kd)_{i,j+1} + (kd)_{i,j}} \frac{T_{i,j+1} - T_{i,j}}{\Delta x}$$

The coefficient is seen with the aid of Fig. 2.2.

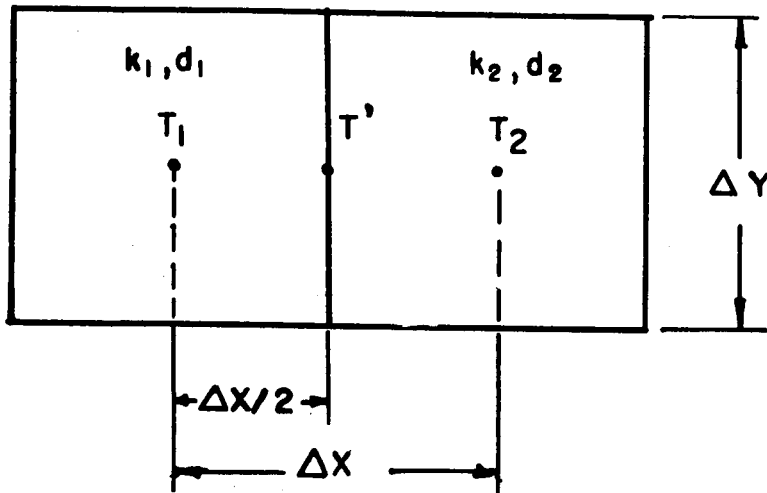


Fig. 2.2. Conductive coupling of adjacent volume elements.

As shown in the figure, a fictitious surface is introduced at the boundary of the two volume elements. The heat flow from T_1 to T' is

$$\Delta y d_1 k_1 \frac{T_1 - T'}{\Delta x/2}$$

and from T' to T_2 is

$$\Delta y d_2 k_2 \frac{T' - T_2}{\Delta x / 2}$$

Since the fictitious surface is not a heat sink or source

$$\Delta y d_1 k_1 \frac{T_1 - T'}{\Delta x / 2} = \Delta y d_2 k_2 \frac{T' - T_2}{\Delta x / 2}$$

and

$$T' = \frac{d_2 k_2 T_2 + d_1 k_1 T_1}{d_2 k_2 + d_1 k_1}$$

Substitution of this expression into the first equation gives for the heat flow from T_1 to T_2

$$\frac{2(k_1 d_1)(k_2 d_2) \Delta y}{d_1 k_1 + d_2 k_2} \frac{T_1 - T_2}{\Delta x}$$

Thus the conduction input per area $\Delta x \Delta y$ becomes

$$\begin{aligned}
& 2(kd)_{i,j} \left[\frac{(kd)_{i-1,j}}{(kd)_{i-1,j} + (kd)_{i,j}} \frac{T_{i-1,j} - T_{i,j}}{\Delta y} \frac{1}{\Delta y} \right. \\
& \cdot \frac{(kd)_{i+1,j}}{(kd)_{i+1,j} + (kd)_{i,j}} \frac{T_{i+1,j} - T_{i,j}}{\Delta y} \frac{1}{\Delta y} \\
& + \frac{(kd)_{i,j-1}}{(kd)_{i,j-1} + (kd)_{i,j}} \frac{T_{i,j-1} - T_{i,j}}{\Delta x} \frac{1}{\Delta x} \\
& \cdot \left. \frac{(kd)_{i,j+1}}{(kd)_{i,j+1} + (kd)_{i,j}} \frac{T_{i,j+1} - T_{i,j}}{\Delta x} \frac{1}{\Delta x} \right] \\
& = \frac{k_1 \left[\frac{T_{i+1,j} - T_{i,j}}{\Delta y} \right]}{\Delta y} - \frac{k_2 \left[\frac{T_{i,j} - T_{i-1,j}}{\Delta y} \right]}{\Delta y} \\
& + \frac{k_3 \left[\frac{T_{i,j+1} - T_{i,j}}{\Delta x} \right]}{\Delta x} - \frac{k_4 \left[\frac{T_{i,j} - T_{i,j-1}}{\Delta x} \right]}{\Delta x}
\end{aligned}$$

Now in the limit the above expression becomes of the form

$$\frac{\partial}{\partial y} \left[K \frac{\partial T}{\partial y} \right] + \frac{\partial}{\partial x} \left[K \frac{\partial T}{\partial x} \right]$$

where

$$K = K(x, y)$$

The radiation factor T^4 can be linearized at $T \approx T_a$ by

$$T^4 = a + b T$$

where

$$a = -3 T_a^4$$

$$b = 4 T_a^3$$

The heat equation for the sensor then can be expressed as

$$\rho c d \frac{\partial T}{\partial t} = \nabla(kd)\nabla T - gT + f \quad (2.1)$$

where

$$g = h_1 + h_2 + 4\sigma T_a^3 (\epsilon_1 + \epsilon_2) \quad (2.2)$$

$$f = h_1 T_{r1} + h_2 T_{r2} + 3\sigma T_a^4 (\epsilon_1 + \epsilon_2) + q_{r1} + q_{r2} + q \quad (2.3)$$

The subscript 1 indicates one side of the sensor and 2 indicates the other side.

Characteristic Time Constant and Equilibrium Temperature

If conduction in the plane of the plate is negligible (as in regions remote from sources and boundaries) the heat equation (Eq. 2.1)

may be written

$$\rho c d \dot{T} = -gT + f$$

where the dot signifies differentiation with respect to time. The equation can further be simplified to the form

$$\tau \dot{T} + T = T_e$$

where

$$\tau = \frac{\rho c d}{g} \quad (2.4)$$

$$T_e = \frac{f}{g} \quad (2.5)$$

thus providing two convenient parameters for reference, the "characteristic time constant" τ and "the equilibrium temperature" T_e .

III. TWO-DIMENSIONAL INTEGRATOR

Finite Difference Method

The finite difference method is used to solve the heat equation by a step-by-step process on the digital computer. The sensor is considered to be overlayed by a rectangular grid. An approximate solution to the differential equation is found at the intersection points of the grid. The solution value $T_{i,j}$ at each grid point represents the temperature of the volume element (i,j) corresponding to that grid point.

The approximation consists of replacing each derivative of the partial differential equation at the grid point, say (i,j) , by a finite difference approximation in terms of the value of T at (i,j) and at neighboring grid points. Similarly, the time derivative is approximated by a finite difference in time.

Explicit Method

A few comments on the simpler explicit method of solving the finite difference equations will serve to introduce the following discussion on the implicit method which was used in the integrator. For this purpose the heat equation (Eq. 2.1) is written as a difference equation

$$(\rho c d)_{i,j} \frac{T_{i,j}^{p+1} - T_{i,j}^p}{\Delta t} = \sum q_c - g_{i,j}^p T_{i,j}^p + f_{i,j}^p \quad (3.1)$$

where

$$\begin{aligned} \sum q_c = & \frac{2(kd)_{i,j}}{\Delta x^2} \left[\frac{(kd)_{i-1,j}}{(kd)_{i,j} + (kd)_{i-1,j}} (T_{i-1,j}^p - T_{i,j}^p) \right. \\ & + \frac{(kd)_{i+1,j}}{(kd)_{i,j} + (kd)_{i+1,j}} (T_{i+1,j}^p - T_{i,j}^p) \\ & + \frac{(kd)_{i,j-1}}{(kd)_{i,j} + (kd)_{i,j-1}} (T_{i,j-1}^p - T_{i,j}^p) \\ & \left. + \frac{(kd)_{i,j+1}}{(kd)_{i,j} + (kd)_{i,j+1}} (T_{i,j+1}^p - T_{i,j}^p) \right] \end{aligned}$$

where

Δx = grid size

Δt = time step

The superscript p indicates the p th time point. Notice that the temperature time increment, $T^{p+1} - T^p$, is explicitly given in terms of temperatures at the preceding time point. Thus,

$$T_{i,j}^{p+1} = T_{i,j}^p + \frac{\Delta t}{\rho c d} \left(\sum q_c - g_{i,j}^p T_{i,j}^p + f_{i,j}^p \right)$$

The size of the grid Δx and the time increment Δt must be carefully chosen to limit the truncation error and numerical error. Suppose D

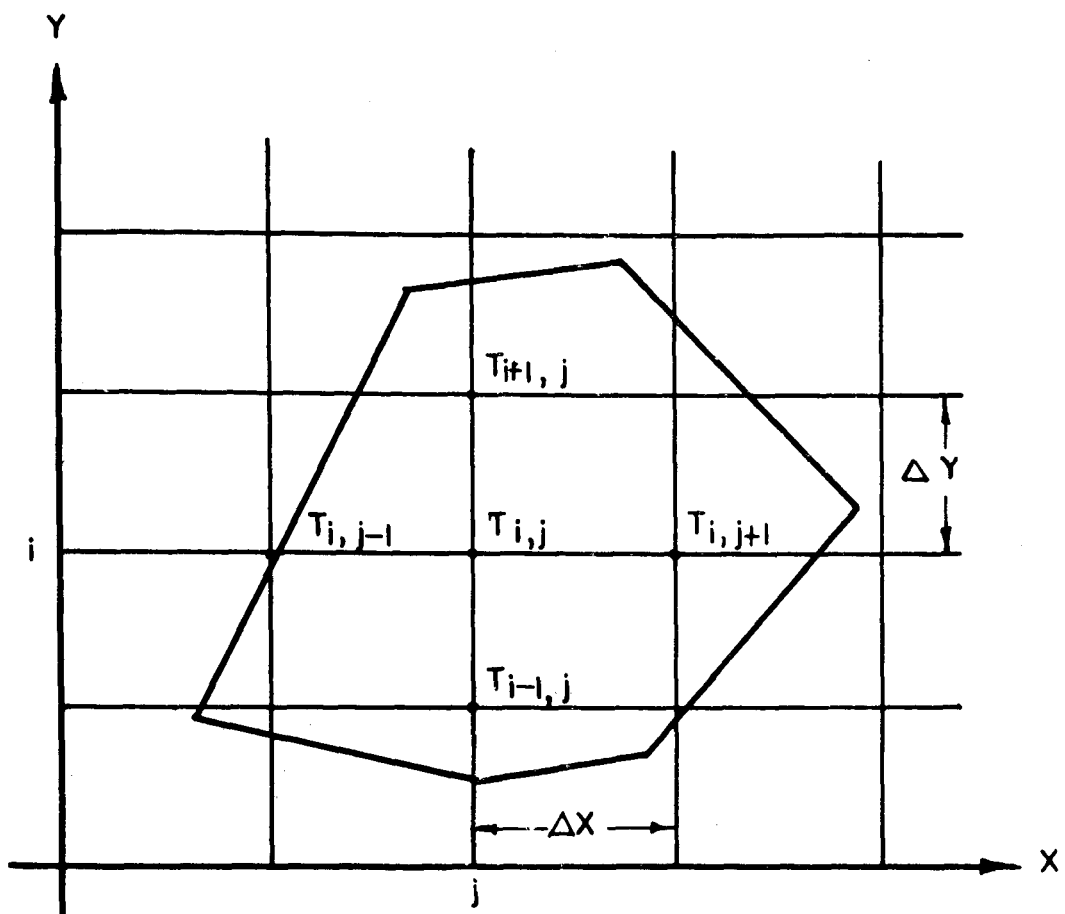


Fig. 3.1. Two-dimensional grid.

represents the exact solution of the partial differential equation,
 Δ represents the exact solution of the partial difference equation,
and N represents the numerical solution of the partial difference
equation. Then $(D - \Delta)$ is called the truncation error; it arises
because of the finite distance between points of the difference mesh.

To find the conditions under which $\Delta \rightarrow D$ is the problem of convergence.

To insure that the difference ($\Delta - N$) is small throughout the entire region of integration is the problem of stability.

There appears to be no appropriate error and stability criteria for the nonlinear equation under study, although it is generally known that larger values of Δx and smaller values of Δt tend to stabilize such systems. [Dusinberre 1961, O'Brien 1951.]

Alternating Direction Implicit Method

Peaceman and Rachford [1955] found an efficient method of solving the linear partial differential equation

$$\frac{\partial T}{\partial t} = R \left[\frac{\partial^2 T}{\partial x^2} + \frac{\partial^2 T}{\partial y^2} \right]$$

Their "alternating direction implicit method" tends to stabilize the system, and a larger Δt can be used. (Actually this method is always stable for the above equation.)

Although the heat equation under study is not a linear equation and otherwise differs from the above equation, the idea of the A-D method is used in this program to solve the heat equation.

Assume the solution is known for time p . The method consists of replacing only one of the second-order derivatives, the derivative in x , say, by an implicit difference approximation, that is, by a finite difference approximation in terms of (unknown) grid values at time $p + 1$.

Previous (known) grid values T^P are used in the second-order derivative in y and in other terms. Therefore, for the time step from p to $p + 1$

$$(\rho cd)_{i,j} \frac{\partial T}{\partial t} = \frac{\partial}{\partial x} \left[(kd)_{i,j} \frac{\partial T}{\partial x} \right]^{p+1} + \frac{\partial}{\partial y} \left[(kd)_{i,j} \frac{\partial T}{\partial y} \right]^p - g_{i,j}^p T_{i,j}^p + f_{i,j}^p \quad (3.2)$$

The advancement of the solution to the $(p + 2)$ th time point is then achieved by using T^{p+2} in the y derivative term and T^{p+1} in the remaining terms.

$$(\rho cd) \frac{\partial T}{\partial t} = \frac{\partial}{\partial x} \left[kd \frac{\partial T}{\partial x} \right]^{p+1} + \frac{\partial}{\partial y} \left[kd \frac{\partial T}{\partial y} \right]^{p+2} - g_{i,j}^{p+1} T_{i,j}^{p+1} + f_{i,j}^{p+1} \quad (3.3)$$

Thus the implicit approximation alternates between x and y components of the conduction expression. After making the finite difference approximations, Eq. 3.2 becomes

$$(\rho cd)_{i,j} \frac{T_{i,j}^{p+1} - T_{i,j}^p}{\Delta t} = \left[\frac{(2kd)_{i,j}}{\Delta x^2} \right] \left[(AKD)_{i,j} (T_{i-1,j}^{p+1} - T_{i,j}^{p+1}) + (BKD)_{i,j} (T_{i+1,j}^{p+1} - T_{i,j}^p) + (CKD)_{i,j} (T_{i,j-1}^{p+1} - T_{i,j}^{p+1}) + (DKD)_{i,j} (T_{i,j+1}^p - T_{i,j}^p) \right] - g_{i,j}^p T_{i,j}^p + f_{i,j}^p$$

where

$$(AKD)_{i,j} = \frac{(kd)_{i-1,j}}{(kd)_{i-1,j} + (kd)_{i,j}}$$

$$(BKD)_{i,j} = \frac{(kd)_{i+1,j}}{(kd)_{i+1,j} + (kd)_{i,j}}$$

$$(CKD)_{i,j} = \frac{(kd)_{i,j-1}}{(kd)_{i,j-1} + (kd)_{i,j}}$$

$$(DKD)_{i,j} = \frac{(kd)_{i,j+1}}{(kd)_{i,j+1} + (kd)_{i,j}}$$

The same procedure can be done for Eq. 3.3, and collecting terms

$$\begin{aligned} P_1 T_{i,j}^{p+1} - P_2 T_{i-1,j}^{p+1} - P_3 T_{i+1,j}^{p+1} &= P_4 T_{i,j}^p + P_5 T_{i,j-1}^p \\ &\quad + P_6 T_{i,j+1}^p + P_7 \end{aligned} \quad (3.4)$$

$$\begin{aligned} Q_1 T_{i,j}^{p+2} - Q_2 T_{i,j-1}^{p+2} - Q_3 T_{i,j+1}^{p+2} &= Q_4 T_{i,j}^{p+1} + Q_5 T_{i-1,j}^{p+1} \\ &\quad + Q_6 T_{i+1,j}^{p+1} + Q_7 \end{aligned} \quad (3.5)$$

where

$$P_1 = (\rho cd)_{i,j} + \frac{\Delta t(2kd)_{i,j}}{\Delta x^2} \left[(AKD)_{i,j} + (BKD)_{i,j} \right]$$

$$P_2 = \frac{\Delta t(2kd)_{i,j}}{\Delta x^2} (AKD)_{i,j}$$

$$P_3 = \frac{\Delta t(2kd)_{i,j}}{x^2} (BKD)_{i,j}$$

$$P_4 = (\rho cd)_{i,j} - \frac{\Delta t(2kd)_{i,j}}{\Delta x^2} \left[(CKD)_{i,j} + (DKD)_{i,j} \right] - g_{i,j}^p$$

$$P_5 = \frac{\Delta t(2kd)_{i,j}}{\Delta x^2} (CKD)_{i,j}$$

$$P_6 = \frac{\Delta t(2kd)_{i,j}}{\Delta x^2} (DKD)_{i,j}$$

$$P_7 = f_{i,j}$$

$$Q_1 = (\rho cd)_{i,j} + \frac{\Delta t(2kd)_{i,j}}{\Delta x^2} \left[(CKD)_{i,j} + (DKD)_{i,j} \right]$$

$$Q_2 = \frac{\Delta t(2kd)_{i,j}}{\Delta x^2} (CKD)_{i,j}$$

$$Q_3 = \frac{\Delta t(2kd)_{i,j}}{\Delta x^2} (DKD)_{i,j}$$

$$Q_4 = (\rho cd)_{i,j} - \frac{\Delta t(2kd)_{i,j}}{\Delta x^2} \left[(AKD)_{i,j} + (BKD)_{i,j} \right] - g_{i,j}^p$$

$$Q_5 = \frac{\Delta t(2kd)}{\Delta x^2} {}_{i,j}^{(AKD)}$$

$$Q_6 = \frac{\Delta t(2kd)}{\Delta x^2} {}_{i,j}^{(BKD)}$$

$$Q_7 = f_{i,j}$$

Expression 3.4 represents $m - 2$ sets of $n - 2$ simultaneous algebraic equations, where $i = 2, 3, 4, \dots, n - 1$ and $j = 2, 3, \dots, m - 1$. Each set of equations is solved to produce the $n - 2$ unknown temperatures based on boundary conditions at $i = 1$ and $i = n$. Gauss' elimination method is used for this purpose. [Forsythe 1960, Bruce 1953.] The temperatures at the next time point are determined from Eq. 3.5 which, in turn, represents $n - 2$ sets of $m - 2$ simultaneous equations.

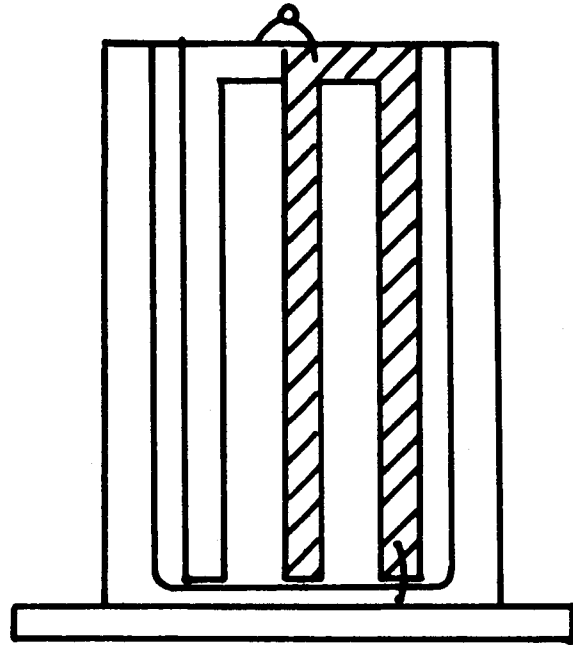
IV. APPLICATION TO ARCASTONDE 1A FILM

The Arcasonde 1A film-mounted bead thermistor is in wide use today for measuring atmospheric temperatures in the stratosphere and mesosphere. The dominating influence of the film on the sensor temperature at the higher altitudes encourages close examination of the thermal behavior of the film in these altitudes. The two-dimensional integrator under discussion offers a useful means of such examination. The properties and configuration of the film are briefly presented along with the environmental parameters associated with an operational flight into the mesosphere (60 and 70 km altitude). From these the quantities g , f , (ρcd) and certain boundary conditions are determined for input to the integrator. Results from the output of the integrator are discussed relative to the performance of the film mount, particularly concerning thermal isolation of support posts, thermal film speed, susceptibility to radiation, and the effect of conduction with the electrical lead wires.

Film Configuration

The film configuration and dimensions are illustrated in Fig. 4.1. The physical properties of the film materials are shown in Table 4.1.

The thermal properties of the film are considered uniform within each of six distinct regions of the film. Arbitrarily choosing one face as the "front" side, we let the subscript $\ell = 1, 2$ designate the front and back side, respectively. Figure 4.2 illustrates the six regions as viewed from the "front" side. We assign the subscript



ARC - 1A

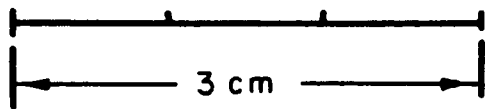


Fig. 4.1. Arcasonde 1A film configuration and dimensions.

TABLE 4.1
Physical Properties Used For The Arcasonde 1A Film

	ρ_c (joul/ $^{\circ}$ K-m 3)	Conductivity (watts/m $^{\circ}$ K)	Emissivity
Mylar	1.75×10^6	23.7×10^{-3}	.80
Silver	2.44×10^6	413.5	.02
Solder	1.20×10^6	52.0	.50

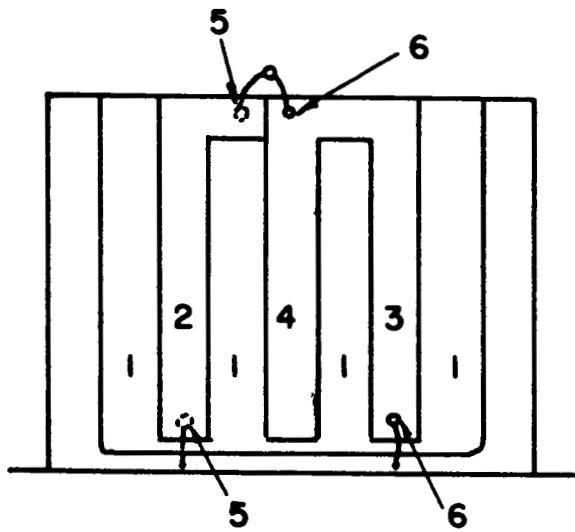


Fig. 4.2. Regions k of the film as seen from the "front" ($l = 1$) side.

$k = 1, \dots, 6$ to the regions as follows:

- $k = 1$ unplated Mylar
- $k = 2$ outer leg (silverplated on back side, "left leg" in Fig. 4.2 and in the program)
- $k = 3$ outer leg (silver-plated on front side, "right leg")
- $k = 4$ inner leg (silver-plated on both sides of the Mylar)
- $k = 5$ junctions (solder, on back side)
- $k = 6$ junctions (solder, on front side)

Radiation Inputs

The radiation environment is considered in four parts, designated as radiant heat sources by the subscript $j = 1, \dots, 4$ as follows:

- $j = 1$ direct solar illumination
- $j = 2$ indirect solar illumination (albedo)
- $j = 3$ earth radiation
- $j = 4$ sonde radiation

The radiation input to an element of the k th region of the film is expressed

$$(q_r)_k = A \sum_{j=1}^4 \sum_{\ell=1}^2 \alpha_{j,k,\ell} f_{j,\ell} I_j \beta_j$$

where

α = radiation absorptivity

f = geometric factor

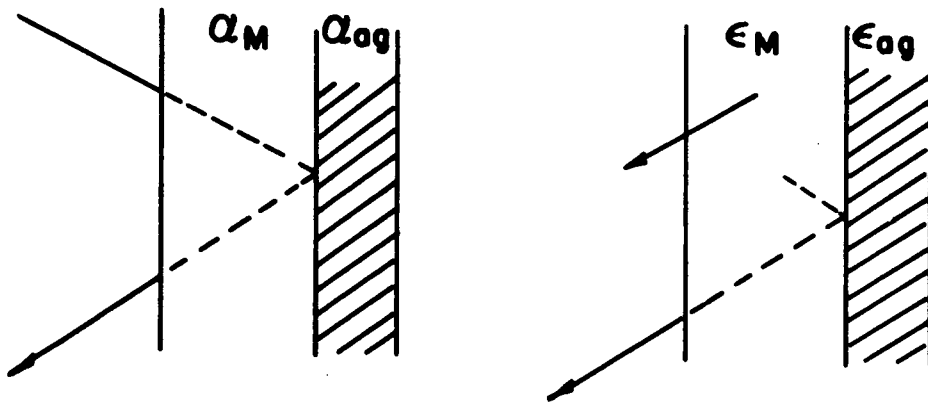
I = radiant emittance

β = perturbation factor

The effective absorptivity of the Mylar-exposed side of a silver-plated region is taken as

$$\alpha = \alpha_M + \left[\alpha_{ag} + \alpha_M (1 - \alpha_{ag}) \right] (1 - \alpha_M)$$

which assumes the reflectivity of the Mylar to be small



and the emissivity as

$$\epsilon = \epsilon_M + (1 - \alpha_M) \left[(1 - \alpha_{ag}) \epsilon_M + \epsilon_{ag} \right]$$

which includes, approximately, the emission of the Mylar forward, that emitted backward and reflected by the silver, and the emission of silver through the Mylar, and which incidentally is the same value as the above absorptivity. Mean solar absorptivities used in the calculations for Mylar, silver, and solder are .0280, 0.01, and 0.5, respectively. Mean long-wave absorptivities were assumed to be 0.451, 0.02, and 0.5, respectively. The resulting absorptivities $\alpha_{j,k,\ell}$ and $\epsilon_{k,\ell}$ are

$$\alpha_{j,k,\ell} = \begin{pmatrix} (.028,.028) (.065,.01) (.01,.065) (.01,.01) (.065,.5) (.5,.065) \\ (.028,.028) (.065,.01) (.01,.065) (.01,.01) (.065,.5) (.5,.065) \\ (.451,.451) (.705,.02) (.02,.705) (.02,.02) (.705,.5) (.5,.705) \\ (.451,.451) (.705,.02) (.02,.705) (.02,.02) (.705,.5) (.5,.705) \end{pmatrix}$$

$$\epsilon_{k,\ell} = \begin{pmatrix} .451 & .451 \\ .705 & .02 \\ .02 & .705 \\ .02 & .02 \\ .705 & .5 \\ .5 & .705 \end{pmatrix}$$

Values used for the geometric factors $f_{j,\ell}$ are

$$\begin{pmatrix} .0000107, 0 \\ .2 , .2 \\ .22 , .22 \\ .02 , .02 \end{pmatrix}$$

which correspond to broadside (strongest) solar illumination of the "front" side of the film, an edge-on (least susceptible) position relative from the earth, and that view of the sonde body seen by the Arcasonde sensor.

Nominal values of source emittance are

$$I_j = \begin{pmatrix} 6.46 \times 10^7 \\ 461. \\ 210. \\ 3.6 \end{pmatrix}$$

The perturbation factor β_j provides a convenient means of producing sun, shade, and night conditions, thus

$$\beta_j = \begin{pmatrix} 1 \\ 1 \\ 1 \\ 1 \end{pmatrix}, \begin{pmatrix} 0 \\ 1 \\ 1 \\ 1 \end{pmatrix}, \begin{pmatrix} 0 \\ 0 \\ 1 \\ 1 \end{pmatrix}$$

represent sunlight, day-shaded, and night-time environments.

Convection Coefficients

The convection coefficient h and recovery factor r depend on altitude, air speed, and distance behind the leading edge of the film [Progress Report, UTEC-MR-67-055, Appendix B]. The functions $h(x)$ and $r(x)$ used as inputs to the integrator are shown in Fig. 4.3.

Conductive Isolation

The integrator computes the time history of temperature at each grid point. If the input to the system is constant, the sensor achieves a steady-state temperature distribution after initial transients have decayed away. Figure 4.4 shows the steady-state distribution at 60 km altitude and 120 m/sec air speed, in daytime shade with an assumed boundary temperature at the support posts of 300°K. The temperature gradient along the flow from the leading edge (top) toward the trailing edge is due to the decrease in h and r downstream on the surface. The distribution is essentially symmetrical about the center flow line. The greater emissivity of Mylar tends to cool the outer legs, relative to the inner leg. The inner leg has no Mylar surface exposed whereas the outer legs expose Mylar on one side. The unplated Mylar is the coolest part of the film, and would tend to cool the edges of the silver plate, though gradients in the plate due to this effect are not apparent.

To illustrate the effect of conduction more clearly, the difference between the steady-state temperature and the local characteristic equilibrium temperature, $(T - T_e)$, is shown in Fig. 4.5. The large temperature difference arising at the junction (solder) regions is due to the

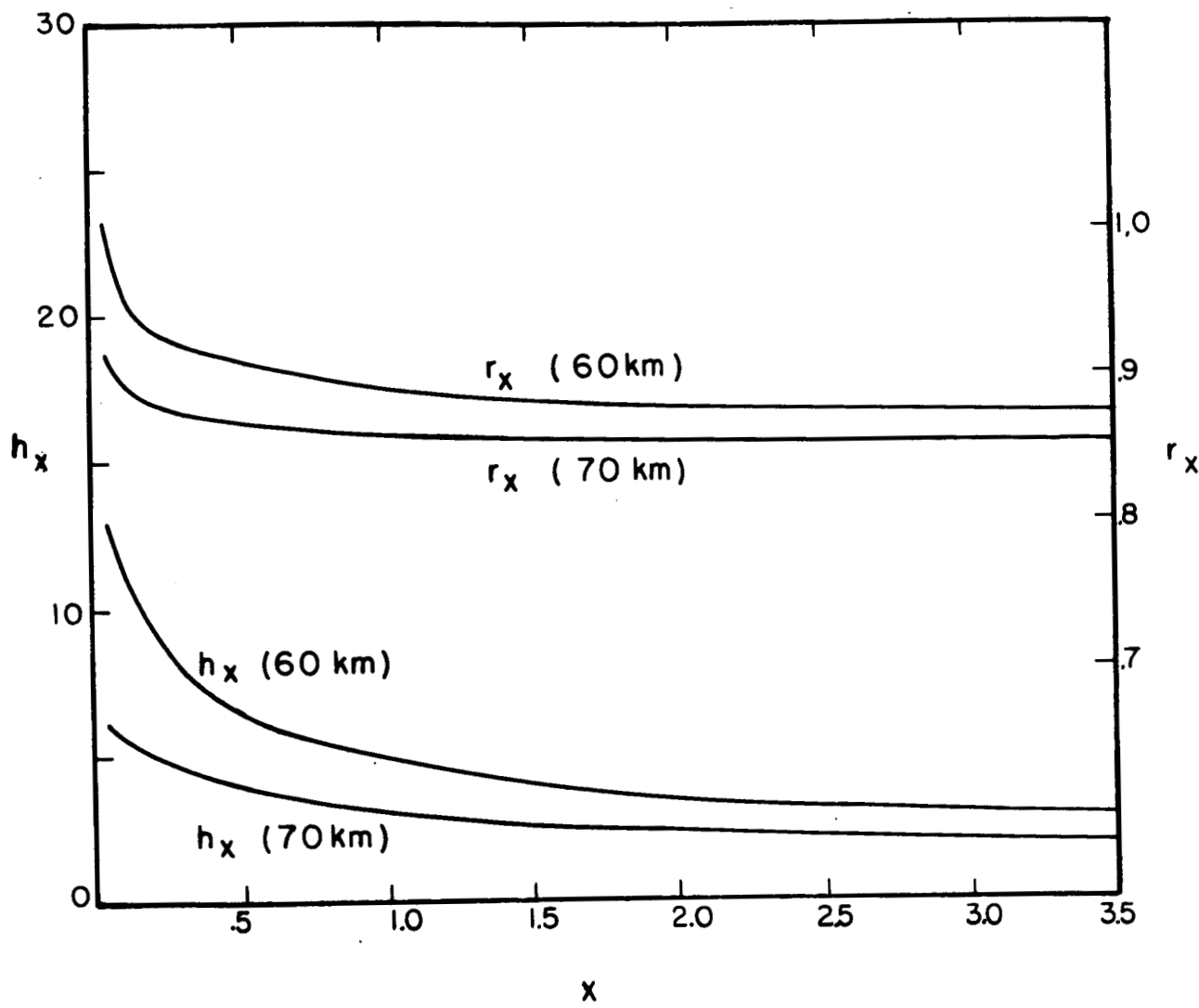
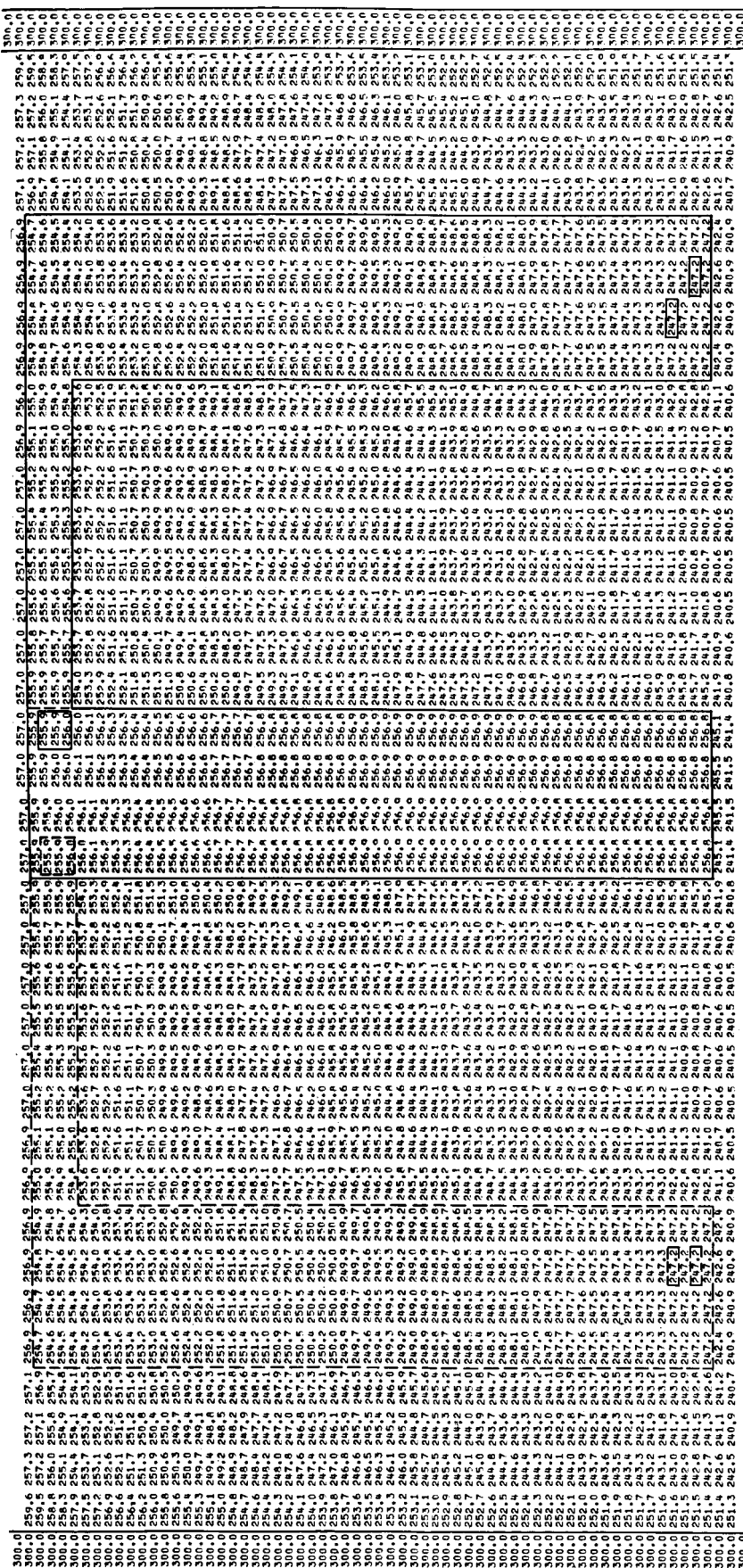


Fig. 4.3. Plots of local convection coefficient h_x (watt/m²°K) and local recovery factor r_x versus distance x (cm) from leading edge for 256 m/sec at 70 km and 120 m/sec at 60 km.

Fig. 4.4. Steady-state temperature distribution at 60 km and 120 m/sec air speed in daytime shade.



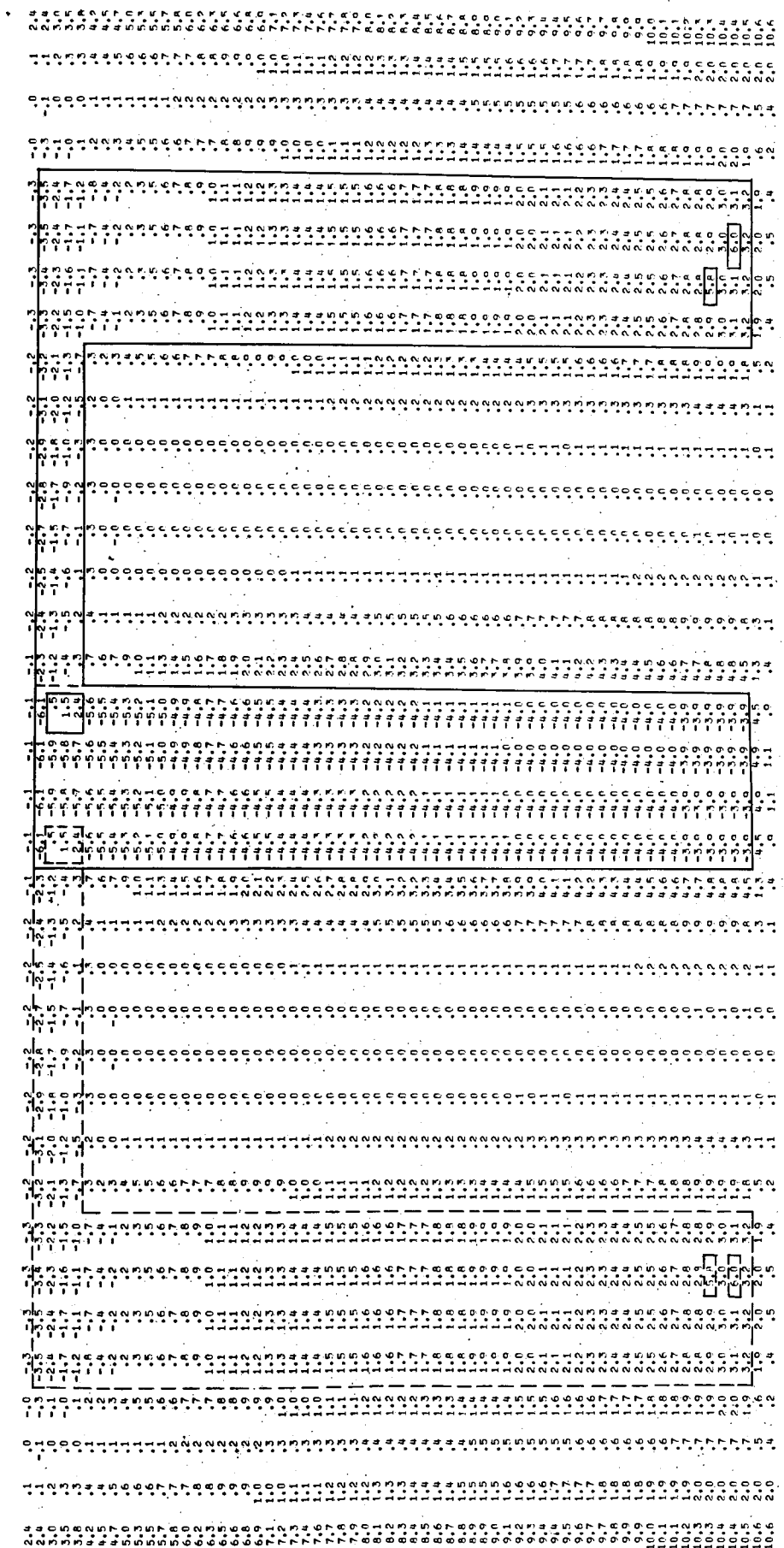


Fig. 4.5. The difference between the steady-state temperature and the local characteristic equilibrium temperature, $(T - T_e)$ (60 km).

difference in T_e between silver and solder. The assumed radiation properties of the solder may be quite inaccurate, so this value is not considered accurate. However, notice in Fig. 4.4 that the junction temperature is unaffected by junction properties anyway, at this altitude. The numbers illustrate the dominance of the silver plate in forcing the junction regions to follow the plate temperature.

Notice that conductive heating of the Mylar is limited to within about two grid elements or one millimeter from a boundary. Figure 4.6 is the result of mathematically disconnecting the film from its supporting posts. Notice the influence of conduction with the posts is nil at the point of contact with the thermistor wires, and, in fact, at all points on the silver plates. It is limited to the 2 mm strip of Mylar along the posts.

Figures 4.7 to 4.9 correspond to the preceding three figures except that the computations are taken at 70 km at 256 m/sec. The decreased convection coefficient h at the higher altitude allows increased conduction effect, but still not enough to affect the wire junctions.

Time Constant

The dynamic response of the film is indicated in Fig. 4.10. The time history of the thermistor wire junction (solder) is shown during the transition from an initially uniform film temperature of 300°K to steady state, under the environments associated with 60 and 70 km altitude. The slight departure from a straight line of the semilog plot is due to the nonlinearity (the fourth power radiation) of the system. An effective

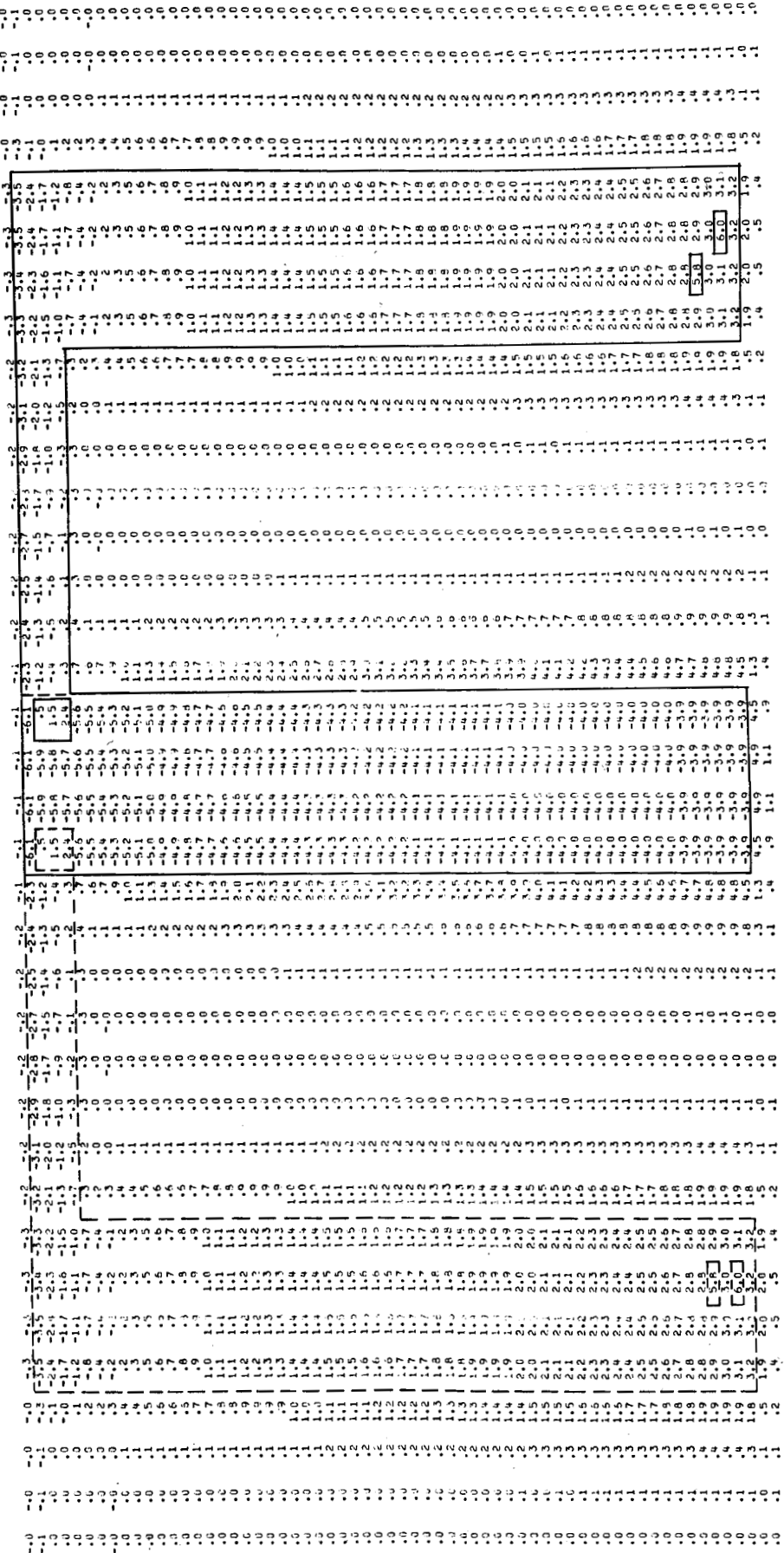
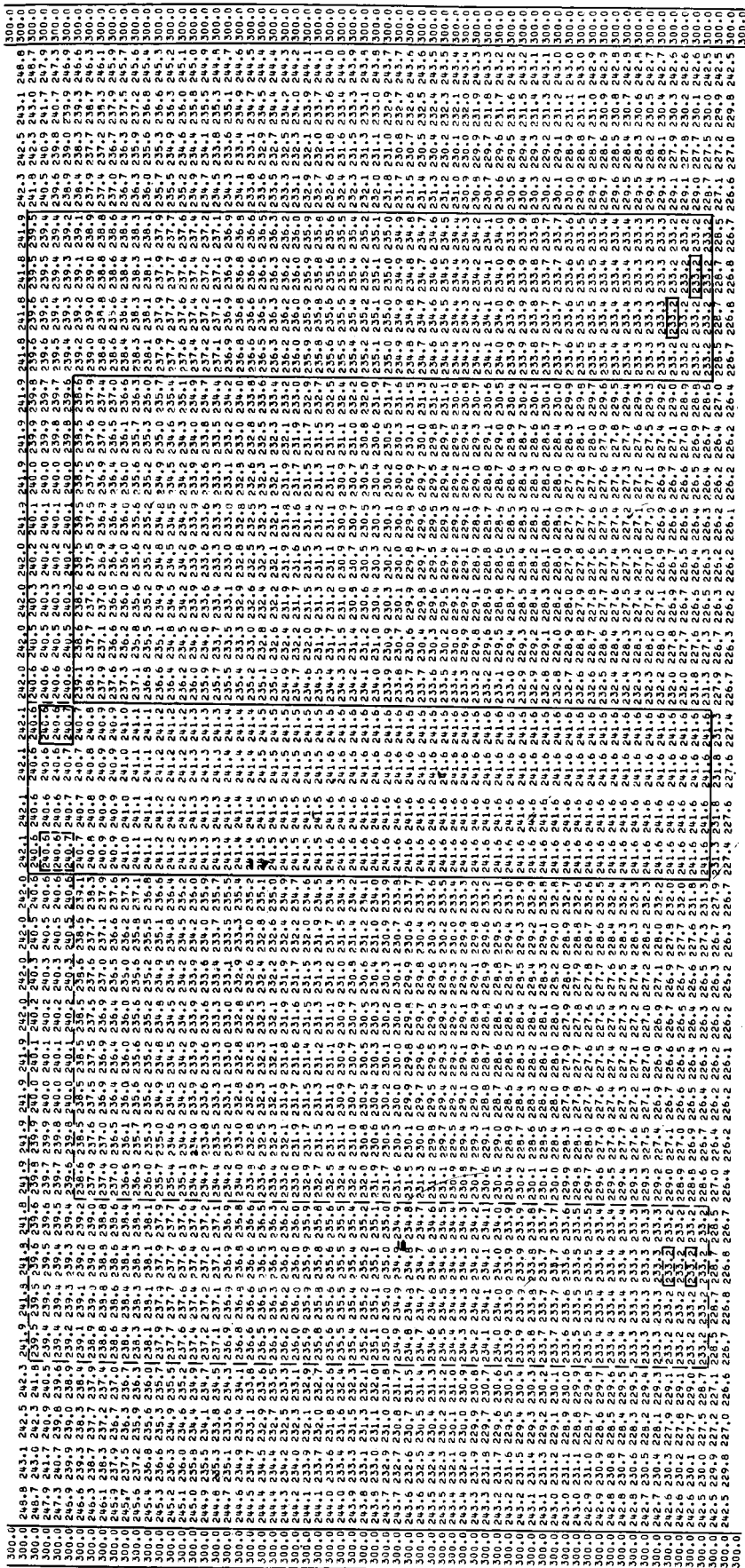
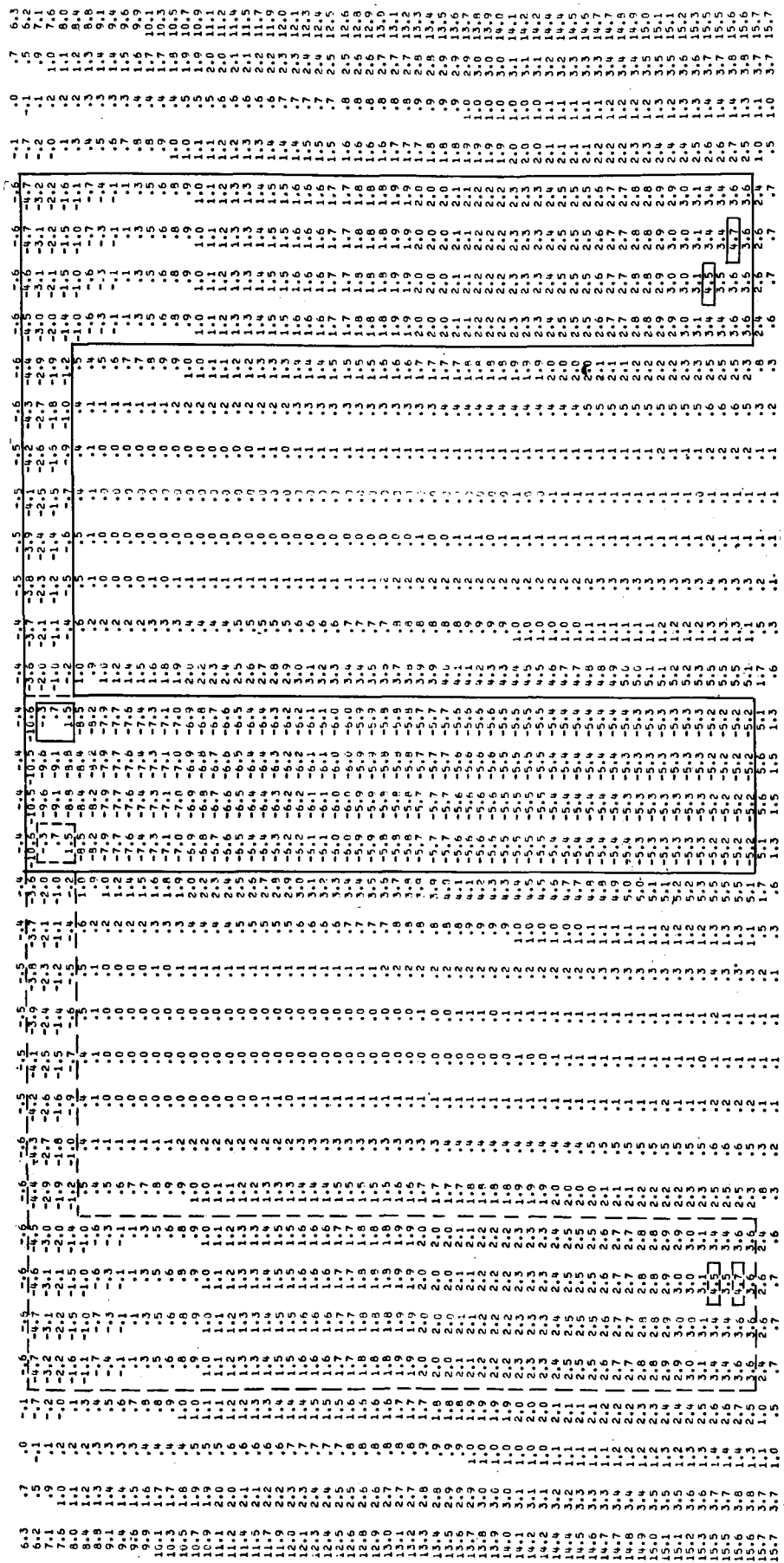


Fig. 4.6. $(T - T_e)$ insulated from support posts (60 km).

Fig. 4.7. Steady-state temperature distribution at 70 km
256 m/sec air speed in daytime shade.

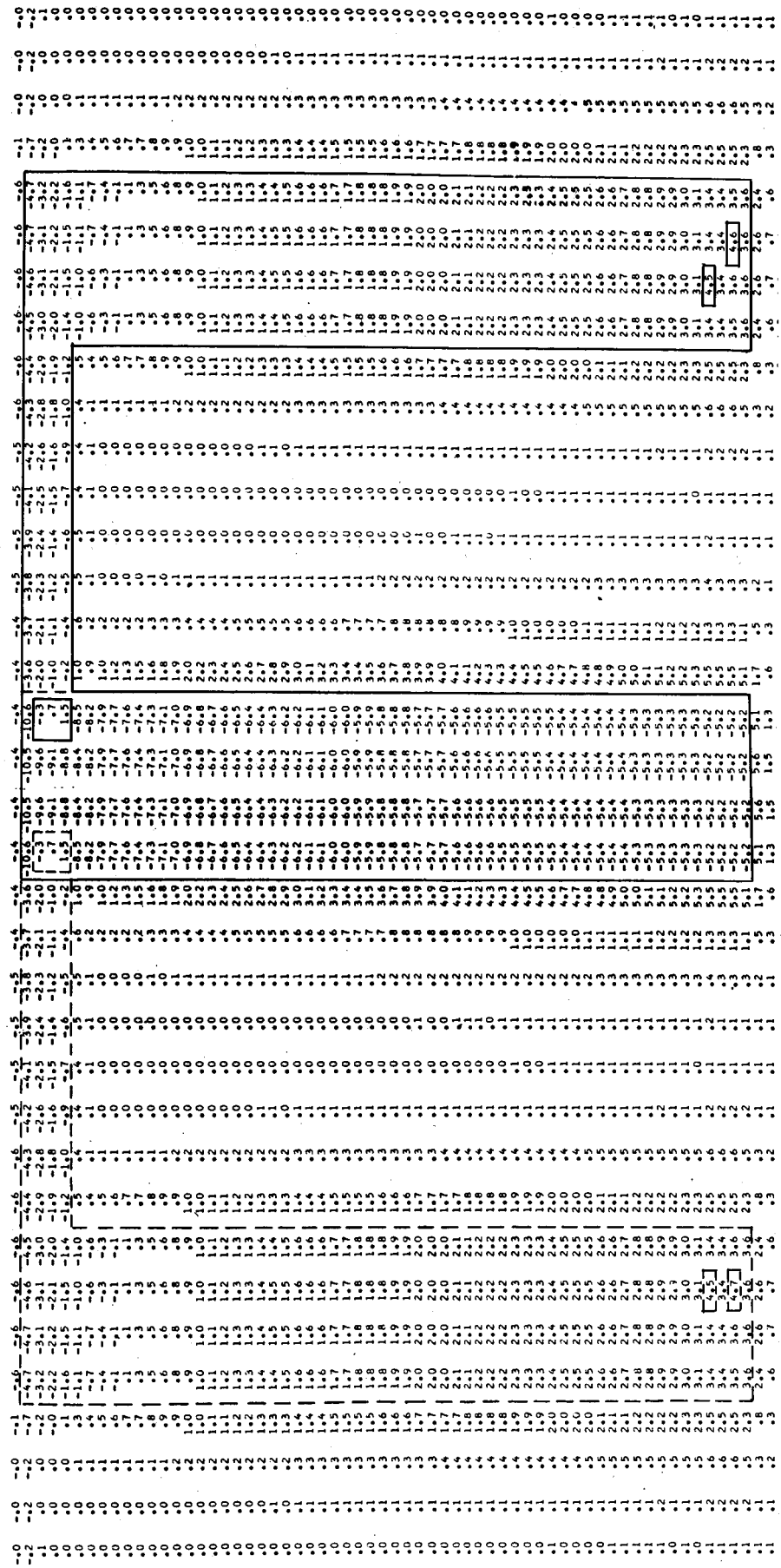




- 33 -

Fig. 4.8. The difference between the steady-state temperature and the local characteristic equilibrium temperature,
 $(T - T_e)$ (70 km),

Fig. 4.9. $(T - T_e)$ insulated from support post (70 km).



time constant may be ascertained, however, as that of a simple first-order system

$$\tau \dot{T} + T = T_e \quad , \quad T(t) = T_e + (T_o - T_e)e^{-t/\tau}$$

which would reach within 10 percent of equilibrium in the same elapsed time. The time constant then is given by

$$\tau = \frac{t_1}{-\ln 0.1} = \frac{t_1}{2.3} \quad , \quad \frac{T(t_1) - T(\infty)}{T(0) - T(\infty)} = 0.1$$

The junction temperature versus time was computed also for the film without solder. The effect of the relatively "massive" solder junctions was found to be essentially nil at 70 km.

Table 4.2 lists the film effective time constant together with the characteristic time constant, pcd/g , calculated at equilibrium and at representative positions on the film, of the junction, silver, and Mylar.

TABLE 4.2

Characteristic Time Constants (pcd/g , seconds) at 70 km, of Junction, Silver (Outer Leg, near Junction), and Mylar (Remote from Silver and Frame), at Beginning ($t = 0$) and End ($t = 50$ sec) of Transient. Also the Effective Time Constant of the Film at the Junction Respectively at 60 and 70 km, and at 70 km Without Solder.

τ (Char.)	$t = 0$	50
Junction	9.0 - 11.1	
Silver	3.4 - 3.9	
Mylar	4.2 - 6.0	
τ (Effective)	$z = 60$	70
Film	4.1	6.52
		6.43
		(w/o solder)

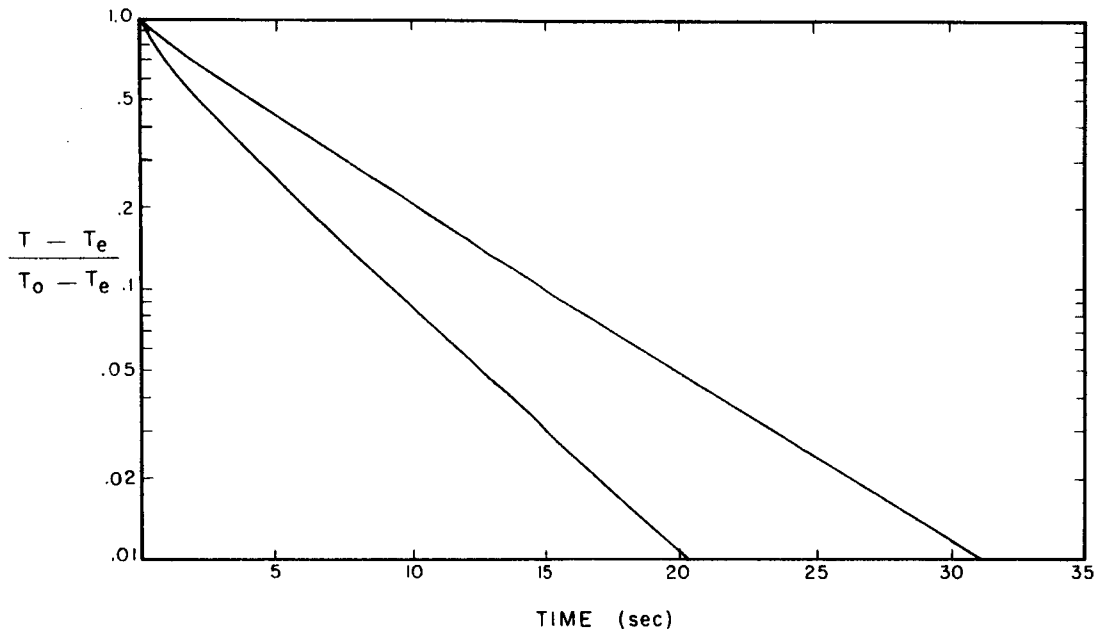


Fig. 4.10. Transient temperature of junction at 60 and 70 km.

Radiation Error

The film temperature dependence on the radiation environment is illustrated in Table 4.3, where the thermistor wire junction temperature is tabulated for the cases of:

- a. Maximum direct solar illumination
- b. Sun-shaded daytime radiation
- c. No solar illumination (night).

Recovery temperature (the sensor equilibrium temperature with no radiation [nor conduction] error) and atmospheric temperature are included in the table as well. Parenthesized quantities indicate successive differences between the given temperatures.

TABLE 4.3

Wire Junction Temperatures when the Film is Under
 (a) Maximum Direct Solar Radiation,
 (b) Sun-shaded Daytime Radiation, and
 (c) No Solar Illumination (Nighttime).

Successive Differences are Parenthesized
 and Recovery and Atmospheric Temperatures are Included for Reference

Altitude (km)	β_j	60	70
T(a)	(1,1,1,1)	257.2 (1.3)	242.9 (2.3)
T(b)	(0,1,1,1)	255.9 (0.3)	240.6 (0.6)
T(c)	(0,0,1,1)	255.6 (-6.5)	240.0 (-10.2)
T_r		262.1 (6.3)	250.2 (30.5)
$T_{(env)}$		255.8	219.7

Notice that the day-night difference in radiant heating, assuming shaded day conditions, is less than 1°K. Since the time constant is significant relative to the period of parachute rotations, the periodic lows of film temperature may be 1 to 2 degrees high due to the persistence of heating from periodic direct solar exposures. The difference in radiation error in the film between day and night flights is less than about 1.5 and 3 degrees, respectively, at 60 and 70 km altitude. It is noted that radiative cooling almost exactly cancels the 6.3°K aerodynamic heating at 60 km.

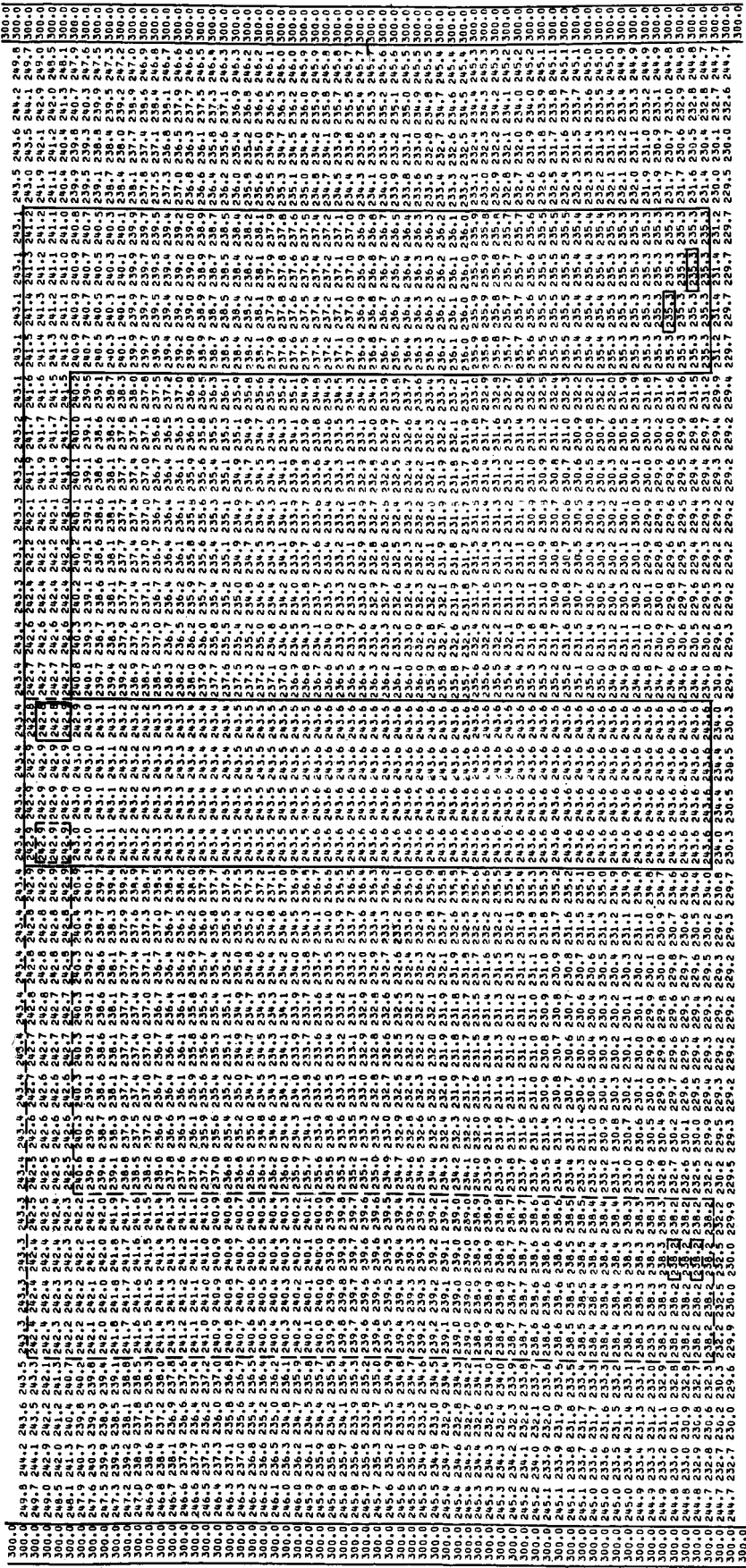
The equilibrium temperature distribution of the film at 70 km under direct solar radiation is given in Fig. 4.11. The sun is illuminating the front side and, therefore, causes the left silver leg (the Mylar-illuminated leg) to be somewhat warmer than the other leg. The difference is small and does not influence the temperature at the sensor wire junction.

Effect of Heat Conduction with the Wires

The above results do not include the effect of conduction with the wires at the junction points. To show the influence of the wires as heat sources or sinks, a computation was completed with heat added at these points.

The heat flow between the thermistor wire and the film may be estimated by calculating the heat flow at the end of a wire having the film temperature at the junction end and the bead temperature at the opposite end. Since the wire length is short, an adequate approximation is given by neglecting radiation and convective heat transfer along the

Fig. 4.11. The equilibrium temperature distribution of the film at 70 km under direct solar radiation.



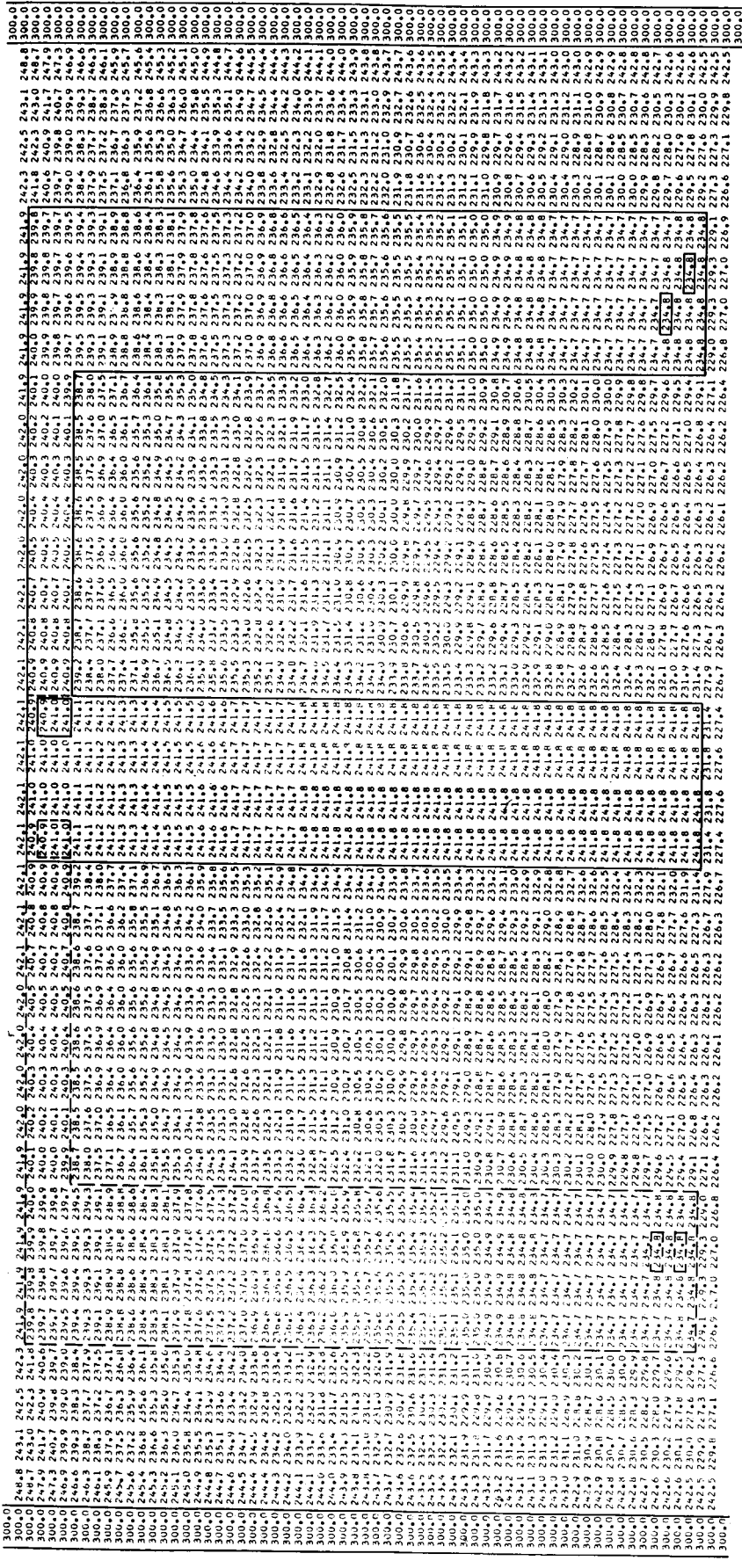
wire. The heat flow per unit bead-film temperature difference is then

$$\frac{q_{wf}}{\Delta T} = \frac{\pi}{4} \frac{k_w d_w^2}{\ell} = \frac{\pi}{4} \frac{(31 \text{ watt/m}^\circ\text{K}) (2.5 \times 10^{-5} \text{ m})^2}{(3.2 \times 10^{-3} \text{ m})} = 4.76 \mu\text{watt/wire } ^\circ\text{K}$$

where the values are those of 1 mil Pt-Ir wire 3.2 mm long. Estimating the maximum temperature difference to be of the order of $10 \pm 5^\circ\text{K}$, an upper bound of $\Delta T = 20^\circ\text{K}$ is chosen which implies an upper limit of about 100 μwatts for each wire.

The wires leading to the sonde are assumed to be the same material but twice the diameter and twice the length. Using an estimated film-sonde temperature difference of about 40°K implies a heat input of about 400 μwatt for each sonde wire.

The effect of this excessive heat input is illustrated in Fig. 4.12. Comparing with Fig. 4.7, it is seen that the temperature rise of the junction is about 0.3°K . The dissipative power of the silver plate is sufficient to render essentially insignificant the heat input from the sensor wire.



- 41 -

Fig. 4.12. Temperature distribution with heat input at wire junctions (70 km).

V. INTEGRATOR PROGRAM

Fortran V was used to program the implicit method discussed in Chapter III. The organization of the programming is summarized in the flow diagram of Fig. 5.1.

In the main program the grid size Δy , dimensions of the plate, time increment of computation Δt , and the required number of iterations are stored. After the initial temperature distribution is stored, subroutine SENSOR is called. Thermal properties of the plate (film configuration) are assigned in subroutine SENSOR.

The environmental conditions are established in subroutine ENVIRO. The value of h , T_r , and radiation input are computed.

Returning to the main program, the first step in LOOP1 is to calculate f and g according to Eq. 2.2. Then COMP1 is called to integrate the time step p to $p + 1$. Resulting values of $T(x, y, p + 1)$ are printed out. Then GANDF is called again to calculate f and g with $T(x, y, p + 1)$, since f and g are functions of T . Then COMP2 integrates the time from $p + 1$ to $p + 2$ to complete the second step in the alternating direction implicit method. $T(x, y, p + 2)$ is then printed out.

LOOP1 is repeated until the temperature distribution reaches equilibrium. Then T_e and ΔT are calculated and are printed out.

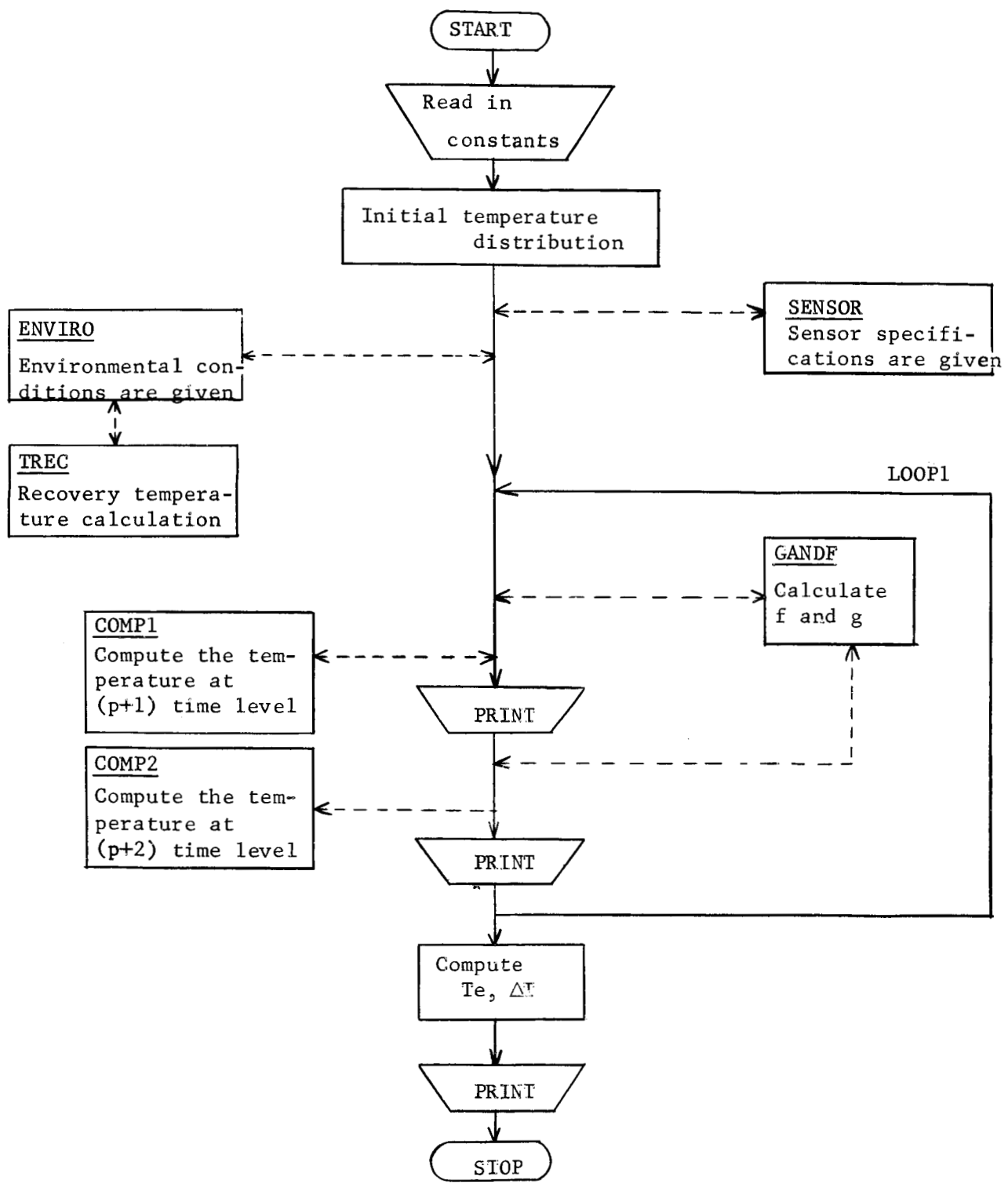


Fig. 5.1. Flow diagram.

MAIN PROGRAM

```

1*      DIMENSION T(65,38),GG(65,38),FF(65,38),AKD(65,38),BKD(65,38),
2*      ICKD(65,38),DKD(65,38), ROC(65,38),H1(65),TR1(65),
3*      C....NUMERICAL CONSTANTS
4*      MM=65
5*      NN=38
6*      LOI=50
7*      DELT=5
8*      DELX=.01/20.
9*      AH=DELX
10*     C....INITIAL TEMPERATURE
11*     DO 1 I=1,MM
12*     DO 1 J=1,NN
13*     T(I,J)=300.
14*     1 CONTINUE
15*     C....FTIM DEFINITION
16*     CALL SENSOR(DELX,T,AKD,BKD,CKD,DKD,ROC,MM,NN,E1,E2,E3,E4,E5,IB0)
17*     C....ENVIRONMENT (H1,H2,TR1,TR2,GR1,GR2,GR3,GR4,GR5L,GR5R,IRO)
18*     INDO=0
19*     C....LOOP 1.....*****.*****.*****.*****.*****.*****.*****.*****.*****.
20*     DO 2 INDE=1,LOL
21*     C....INTEGRATION P+1
22*     CALL GANDF(H1,H2,TR1,TR2,GR1,GR2,GR3,GR4,FF,GG,T,E1,E2,E3,E4,IND,
1MM,NN,E5,GR5L,GR5R,IB0)
23*     CALL COMP(AKD,BKD,CKD,DKD,GG,AHH, ROC,FF,T,DELX,DELT,MM,NN)
24*     C....SELECTED OUTPUTS TRANSIENT
25*     T1=FF(40,13)/GG(40,13)
26*     TAU1=ROC(40,13)/GG(40,13)
27*     TT2=FF(5,17)/GG(5,17)
28*     TAU2=ROC(5,17)/GG(5,17)
29*     TT3=FF(5,18)/GG(5,18)
30*     TAU3=ROC(5,18)/GG(5,18)
31*     TT4=FF(5,21)/GG(5,21)
32*     TT5=FF(40,4)/GG(40,4)
33*     TT6=FF(6,32)/GG(6,32)
34*     TAU4=ROC(6,18)/GG(6,18)
35*     TT7=FF(5,16)/GG(5,16)
36*     PRINT 105,IND,GG(40,13),FF(40,13),TAU1,GG(5,17),FF(5,
37*     TT1=FF(5,17),TAU2
38*     PRINT 106,TT1,TT5,TAU1,TT4,T(5,21),TT5,T(40,4),TT6,T(61,32),T(
39*     140,32),T(40,19),T(40,7)
40*     C....INTEGRATION P+2
41*     CALL GANDF(H1,H2,TR1,TR2,GR1,GR2,GR3,GR4,FF,GG,T,E1,E2,E3,E4,IND,
1MM,NN,E5,GR5L,GR5R,IB0)
42*     CALL COMP2(AKD,BKD,CKD,DKD,GG,AHH, ROC,FF,T,DELX,DELT,MM,NN)
43*     C....SELECTED OUTPUTS TRANSIENT
44*     TT1=FF(40,13)/GG(40,13)
45*     TAU1=ROC(40,13)/GG(40,13)
46*     TT2=FF(5,17)/GG(5,17)
47*     TAU2=ROC(5,17)/GG(5,17)
48*     TT3=FF(5,18)/GG(5,18)
49*     TT4=FF(5,21)/GG(5,21)
50*     TT5=FF(40,4)/GG(40,4)
51*     TT6=FF(6,32)/GG(6,32)
52*     TAU3=ROC(5,18)/GG(5,18)
53*     TT7=FF(5,16)/GG(5,16)
54*     PRINT 105,IND,GG(40,13),FF(40,13),TAU1,GG(5,17),FF(5,
55*     117),TT2,T(5,17),TAU2
56*     PRINT 106,TT3,T(5,18),TAU3,TT4,T(5,21),TT5,T(40,4),TT6,T(61,32),T(
57*     140,32),T(40,19),T(40,7)
58*     2 CONTINUE
59*     C....LOOP 1.....*****.*****.*****.*****.*****.*****.*****.*****.*****.
60*     C....PRINT OUTPUT EQUILIBRIUM
61*     PRINT 101
62*     PRINT 102,IND
63*     PRINT 103,((TI,J),J=1,19),I=1,65)
64*     PRINT 103,((TI,J),J=20,38),I=1,65)

C....CALCULATION OF TE
65*     DO 3 I=1,MM
66*     DO 3 J=1,NN
67*     3 FF(I,J)=FF(I,J)/GG(I,J)
68*     PRINT 103,((FF(I,J),J=1,19),I=1,65)
69*     PRINT 103,((FF(I,J),J=20,38),I=1,65)
70*     C....CONDUCTION ERROR
71*     72*     DO 4 I=1,MM
72*     DO 4 J=1,NN
73*     4 GG(I,J)=T(I,J)-FF(I,J)
74*     PRINT 103,((GG(I,J),J=1,19),I=1,65)
75*     PRINT 103,((GG(I,J),J=20,38),I=1,65)
76*     77*     100 FORMAT(1H ,15,6,1,E10,4,2F6.,,E10,4,5F6,1)
77*     101 FORMAT(40H ,COMPUTED RESULTS
78*     102 FORMAT(1H ,4HIND=,13)
79*     103 FORMAT(1H ,19F6,1)
80*     104 FORMAT(40H ,ANALYTICAL RESULTS
81*     105 FORMAT(1H ,15,F6,1,E10,4,4F6,1,E10,4,3F6,1)
82*     106 FORMAT(1H ,12F6,1)
83*     STOP
84*   END
85* 
```

SUBROUTINE SENSOR

```

1* SUBROUTINE SENSOR(DELX,T,AKD,BKD,CKD,DKD, ROC(MM,NN,E1,E2,E3,E4,E5
2* 1,IO)
3* DIMENSION T(65,38),AKD(65,38),BKD(65,38),CKD(65,38),DKD(65,38),ROC
4* 1(65,38),COC(65,38)
5* MM=MM-1
6* NN=NN-1
7* C..... COMPONENT PROPERTIES
8* EML1=.151
9* ESILV=.02
10* DSOLD=.5
11* ALMYL=.5
12* ALSILV=.051
13* ALSOLD=.050
14* DMYL=.25*E-6
15* DSILV=.05*E-6
16* DSOLD=.89*E-6
17* CMYL=.3*6E-3
18* CSILV=.413*478
19* CSOLD=.52
20* RCMYL=.1*7.45E6
21* RSILV=.2*44E6
22* RSOLD=.1*2E6
23* C..... FILM REGION PROPERTIES
24* E1=EMYL
25* E2=EMYL+(1.-ALMYL)*(1.-ALSILV)*ENYL*ESILV
26* E3=ESILV
27* E4=ESOLD
28* DK1=DNYL*CMYL
29* DK2=DMYL*CMYL
30* DK3=DK2
31* DK4=DNYL*MYL+(DNL*CSILV)*2.
32* ROC1=RCMYL*DMYL
33* ROC2=RCMYL*DMYL+RCSTLV*DSILV
34* ROC3=ROC2
35* ROC4=RCMYL*DMYL*2.* (RCSTLV*DSILV)
36* C..... FILM CONFIGURATION
37* C..... MYLAR PART
38* DO 1 I=1,MM
39* DO 1 J=1,NN
40* COC (I,J)=DK1
41* 1 ROC (I,J)=ROC1
42* C..... LEFT LEG
43* DO 2 J=6,9
44* DO 2 I=3,62
45* COC (I,J)=DK2
46* 2 ROC (I,J)=ROC2
47* DO 3 I=3,6
48* DO 3 J=0,17
49* COC (I,J)=DK3
50* 3 ROC (I,J)=ROC3
51* C..... INNER LEG
52* DO 4 I=1,62
53* DO 4 J=18,21
54* COC (I,J)=DK4
55* 4 ROC (I,J)=ROC4
56* C..... RIGHT LEG
57* DO 5 I=3,6
58* DO 5 J=22,29
59* COC (I,J)=DK3
5 ROC (I,J)=ROC3
60* 5 ROC (I,J)=ROC3
61* DO 6 I=3,62
62* DO 6 J=30,33
63* COC (I,J)=DK3
64* 6 ROC (I,J)=ROC3

```

SUBROUTINE ENVIRO

```

1.1* SUBROUTINE ENVIRO (H1,H2,TR1,TR2,GR1,GR2,GR3,GR4,GR5,L,GR5R,IB0)
1.2* DIMENSION F(5,2),ALF(6,6,2),BET(5),AI(5),H1(65),H2(65)
1.3* C..... VALUE OF H AND TR
1.4* CALL TREC(TR1)
1.5* READ 135,(H1(I),I=1,65)
1.6* H1(1)=H1(2)
1.7* C..... RADIATION INPUT
1.8* READ 100,(F(J,J),J=1,4)
1.9* READ 100,(F(J,J),J=1,4)
1.9* READ 101,((ALF(I,J,K),K=1,6),J=1,4)
1.9* READ 101,((ALF(I,J,K),K=1,6),J=1,4)
1.9* READ 102,((BET(I,J),J=1,4)
1.9* READ 103,(AI(I,J),J=1,4)
1.9* READ 103,(AI(I,J),J=1,4)
1.9* 2 CONTINUE
1.9* QRI=0.0
1.9* QR2=0.0
1.9* QR3=0.0
1.9* QR4=0.0
1.9* QR5=0.0
1.9* QR5R=0.0
1.9* D0 1 L21,2
1.9* DO 1 J=1,4
1.9* GRI=GR1+F(J,L)*ALF(J,1,L)*BET(J,J)*AI(J)
1.9* GR2=GR2+F(J,L)*ALF(J,2,L)*BET(J,J)*AI(J)
1.9* GR3=GR3+F(J,L)*ALF(J,3,L)*BET(J,J)*AI(J)
1.9* GR4=GR4+F(J,L)*ALF(J,4,L)*BET(J,J)*AI(J)
1.9* GR5=GR5+F(J,L)*ALF(J,5,L)*BET(J,J)*AI(J)
1.9* QRA=GR5R*(F(J,L)*ALF(J,6,L)*BET(J,J)*AI(J))
1.9* 1 CONTINUE
1.9* C..... PRINT INPUTS
1.9* PRINT 104
1.9* PRINT 105
1.9* PRINT 106,(F(I,L),I=1,2)
1.9* PRINT 107,(F(I,L),I=1,2)
1.9* PRINT 108,(F(I,L),I=1,2)
1.9* PRINT 109,(F(I,L),I=1,2)
1.9* PRINT 110
1.9* PRINT 111
1.9* PRINT 112,((ALF(I,J,K),K=1,4),L=1,2)
1.9* PRINT 113,((ALF(I,J,K),K=1,4),L=1,2)
1.9* PRINT 114,((ALF(I,J,K),K=1,4),L=1,2)
1.9* PRINT 115,((ALF(I,J,K),K=1,4),L=1,2)
1.9* PRINT 116
1.9* PRINT 117,BET(1)
1.9* PRINT 118,BET(2)
1.9* PRINT 119,BET(3)
1.9* PRINT 120,BET(4)
1.9* PRINT 121
1.9* PRINT 122,AI(1)
1.9* PRINT 123,AI(2)
1.9* PRINT 124,AI(3)
1.9* PRINT 125,AI(4)
1.9* PRINT 126
1.9* PRINT 127,GR1
1.9* PRINT 128,GR2
1.9* PRINT 129,GR3
1.9* PRINT 130,GR4
1.9* PRINT 131,GR5
1.9* PRINT 132,GR5L

```

SUBROUTINE TREC

```

1* SUBROUTINE TREC(TR1)
2* DIMENSION TR1(65),RLOC(65)
3* DELX=.01/20.
4* READ 100,AMFP,VEL,RHO,AMU,TINF
5* ALT770,E3
5* DO 40 K=1,62
6* X=DELX*k
7* AMF=AMFP/X
8* AMFRHO*VEL*X/AMU
9* AMKFT=AMKF((SORT(REF))'/7.2
10* REF=.815*(AMKF*.322)/(AMKF+.3)
11* TR=TINF+RFL*VEL*(2.+1012.*6)
12* K=K+2
13* TR1(K)=TR
14* RLOC(K)=RFL
15* CONTINUE
16* TR1(1)=TR1(3)
17* TR1(2)=TR1(3)
18* TR1(65)=TR1(64)
19* C.....PRINT INPUTS
20* PRINT 103
21* PRINT 101,ALT,VEL,TINF
22* PRINT 14
23* PRINT 105*,RLOC(I),I=1,65)
24* 100 FORMAT(1H ,4HALT=,E8.4,4HVEL=,E8.4,5HTINF=,E8.4)
25* 101 FORMAT(1H ,4HVAL=,E8.4,4HVEL=,E8.4,5HTINF=,E8.4)
26* 102 FORMAT(5DH ENVIRONMENTAL VALUE OUTPUT
27* 103 FORMAT(5DH LOCAL R
28* 104 FORMAT(5DH LOCAL R
29* 105 FORMAT(1H ,20F6.1)
30* RETURN
31*

```

```

21* GSENS=100.E-6
22* GSOND=400.E-6
23* GSONDSENS/(3.*#DELX*DELX)
24* GSONDSENS/12.*#DELX*DELX)
25* PRINT 139
26* PRINT 140,(H1(I),I=1,65)
27* 1 CONTINUE
28* C.....HYLR PART
29* DO 2 I=1,MM
30* DO 2 J=1,NN
31* T3(I,J)=T(I,J)*#3
32* FF(I,J)=HT(I)+SIG31*T(I,J)*T(I,J)+QR1
33* 2 GG(I,J)=2.*HH1(I)+SIG41*T3(I,J),
34* C.....LEFT LEG (1)
35* DO 3 I=2,62
36* DO 3 J=9
37* FF(I,J)=HT(I)+SIG32*T3(I,J)*T(I,J)+QR2
38* 3 GG(I,J)=2.*HH1(I)+SIG42*T3(I,J),
39* C.....LEFT LEG (2)
40* DO 4 I=2,6
41* DO 4 J=10,17
42* FF(I,J)=HT(I)+SIG32*T3(I,J)*T(I,J)+QR2
43* 4 GG(I,J)=2.*HH1(I)+SIG42*T3(I,J),
44* C.....INNR LEG
45* DO 5 I=1,62
46* DO 5 J=18,21
47* FF(I,J)=HT(I)+SIG44*T3(I,J)*T(I,J)+QR4
48* 5 GG(I,J)=2.*HH1(I)+SIG44*T3(I,J),
49* C.....RIGHT LEG (1)
50* DO 6 I=2,6
51* DO 6 J=22,29
52* FF(I,J)=HT(I)+SIG33*T3(I,J)*T(I,J)+QR3
53* 6 GG(I,J)=2.*HH1(I)+SIG33*T3(I,J),
54* C.....RIGHT LEG (2)
55* DO 7 I=1,62
56* DO 7 J=20,33
57* FF(I,J)=HT(I)+SIG33*T3(I,J)*T(I,J)+QR3
58* 7 GG(I,J)=2.*HH1(I)+SIG33*T3(I,J),
59* C.....WIRE JUNCTION
60* DO 8 I=1,6
61* FF(I,1,21)=HT(I)+SIG135*T3(I,21)*T(I,21)+QR5R+QR1
62* 8 GG(I,1,21)=2.*HH1(I)+SIG135*T3(I,21)
63* FF(I,9,31)=HT(I,5)+SIG35*T3(159,31)*T(59,31)+QR5R+QR2
64* FF(I,6,32)=HT(I,6)+SIG35*T3(161,32)*T(61,32)+QR5R+QR2
65* GG(59,31)=2.*HH1(59)+SIG45*T3(59,31)
66* GG(61,32)=2.*HH1(61)+SIG45*T3(61,32)
67* DO 9 I=1,6
68* FF(I,1,18)=HT(I)+SIG135*T3(I,18)*T(I,18)+QR5L+QR1
69* 9 GG(1,18)=2.*HH1(I)+SIG135*T3(I,18)
70* DO 10 I=59,61,2
71* FF(I,8,HT(I,8)+SIG35*T3(I,8)*T(I,8)+QR5L+QR2
72* 10 GG(I,8)=2.*HH1(I,8)+SIG45*T3(I,8),
73* 139 FORMAT(25H VALUE OF H
74* 140 FORMAT(1H ,20F6.2)
75* RETURN
76* END

```

SUBROUTINE GANDF

```

1* SUBROUTINE GANDF(H1,H2,TR1,TR2,QR1,QR2,QR3,QR4,FF,GG,T,E1,E2,E3,E4
2* 1,IND,MMN,ES,GS5,GR5,IR5,IR6)
3* DIMENSION FF(165,38),GG(165,38),ES(165,38),IR5(165,38),IR6(165,38)
4* DIMENSION H1(65),HT(65),TR1(65)
5* IF(LIND,GT,1) GO TO 1
6* SIGM5=.6*E8
7* DO 11 I=1,65
8* H(I)=2.*HH1(I)*TR1(I)
9* SIG41=SIGM**.**(E1+E1)
10* SIG42=SIGM**.**(E2+E2)
11* SIG4=SIG42
12* SIG44=SIGM**.**((E3+E3)
13* SIG45=SIGM**.**((E2+E4)
14* SIG3=SIGM**.**((E2+E4)
15* SIG32=SIGM32
16* SIG33=SIGM33
17* SIG34=SIGM**.**((E3+E3)
18* SIG35=SIGM**.**((E2+E4)
19* C.....HEAT INPUT
20* DELX=.01/20.
```

SUBROUTINE COMP1

```

1* SUBROUTINE COMP1(AKD,BKD,CKD,DKD,GG,AHH, ROC,FF,T,DELX,DELTA,MM,
1NN)
2* DIMENSIONAKD(65,38),BKD(65,38),CKD(65,38),DKD(65,38),GG(65,38),
3* IFF(65,38),A(65),B(65),C(65),D(65),ODK(65),CC(65),BBK(65),T(65,38),
4* 2,U(65,38),ROC(65,38)
5* MM1=MM-1
6* NN1=NN-1
7* MM2=MM-2
8* NN2=NN-2
9* BENN=AHH*AHH
10* BENR=+*AHH*AHH
11* DDD=DELX*DELX/DELT A
12* DO 3 J=2,NN1
13* DO 2 I=2,MM1
14* FACT=ROC(I,J)*DDD
15* A(I)=+AKD(I,J)
16* B(I)=BKD(I,J)+AKD(I,J)+BENR*GG(I,J)+FACT
17* C(I)=BKD(I,J)
18* D(I)=CKD(I,J)+DKD(I,J)+BENR*GG(I,J)+FACT
19* D(1)=CKD(1,J)*T(1,J-1)-D1*(T(1,J)-DKD(1,J))*T(1,J+1)+BENN*FF(1,J)
20* D(2)=D(1)+AND(2,J)*(T(1,J)
21* D(MM1)=D(1)+BKD(MM1,J)*T(MM1,J)
22* IF(I,.E.,3) GO TO 1
23* CCK(I)=C(I)/B(I)
24* DOK(I)=D(I)/B(I)
25* DOK(I)=D(I)/B(I)
26* GO TO 2
27* 1 BBK(1)=B(1)-A(1)*CCK(I-1)
28* CCK(I)=C(I)/BBK(I)
29* DOK(I)=(D(I)-A(I))/DDK(I-1)/BBK(I)
30* 2 CONTINUE
31* U(MM1,J)=DDK(MM1)
32* DO 3 K=2,MM2
33* TI=MM-K
34* U(TI,J)=DDK(TI)-CCK(TI)*U(TI+1,J)
35* 3 CONTINUE
36* DO 4 J=2,NN1
37* DO 4 I=2,MM1
38* T(I,J)=U(I,J)
4* T(I,J)=U(I,J)
RETURN
END

```

SUBROUTINE COMP2

```

1* SUBROUTINE COMP2(AKD,BKD,CKD,DKD,GG,AHH, ROC,FF,T,DELX,DELTA,MM,
1NN)
2* DIMENSIONAKD(65,38),BKD(65,38),CKD(65,38),DKD(65,38),GG(65,38),
3* IFF(65,38),A(65),B(65),C(65),D(65),ODK(65),CC(65),BBK(65),T(65,38),
4* 2,U(65,38),ROC(65,38)
5* MM1=MM-1
6* NN1=NN-1
7* MM2=MM-2
8* NN2=NN-2
9* DDD=DELX*DELX/DELT A
10* BEIN=AHH*AHH
11* BEFR=+*AHH*AHH
12* DO 3 I=2,MM1
13* DO 2 J=2,NN1
14* FACT=ROC(I,J)*DDD
15* A(J)=+CKD(I,J)
16* B(J)=DKD(I,J)+CKD(I,J)+REN R*GG(I,J)+FACT
17* C(J)=DDK(I,J)
18* D(J)=AKD(I,J)*BKD(I,J)+BENR*GG(I,J)-FACT
19* D(I)=AKD(I,J)*T(I,J-1)
20* D(1)=D(0)+COK(1,2)*T(1,J)
21* D(NN1)=D(0)+OKD(1,NN1)*T(1,NN)
22* IF (.L.GE.,3) GO TO 1
23* CCK(J)=C(J)/B(J)
24* DOK(J)=D(J)/B(J)
25* DOK(J)=D(J)/B(J)
26* GO TO 2
27* 1 BBK(J)=B(J)-A(J)*CCK(J-1)
28* CCK(J)=C(J)/BBK(J)
29* DOK(J)=(D(J)-A(J))/DDK(J-1)/BBK(J)
30* 2 CONTINUE
31* U(1,NN1)=DDK(NN1)
32* DO 3 K=2,NN1
33* JJ=NN-K
34* U(JJ,J)=DDK(JJ)-CCK(JJ)*U(J,J+1)
35* 3 CONTINUE
36* DO 4 J=2,NN1
37* DO 4 I=2,MM1
38* T(I,J)=U(I,J)
4* T(I,J)=U(I,J)
RETURN
END

```

Main Program

Line

4-5 MM,NN : numbers of grid points in x and y
6 LOL : number of iterations to be made to reach
 equilibrium
7 DELTA : time step (Δt)
8 DELX : grid size (Δx)
13 T(I,J) : (i-j)th grid point temperature
20 LOOP1 is repeated LOL times to reach equilibrium
26-39 FF(I,J),GG(I,J) : $f_{i,j}$ and $g_{i,j}$
 ROC(I,J) : $(\rho cd)_{i,j}$
 Calculation of $T_e = f/g$, $\tau = \rho cd/g$
59 End of LOOP1
68 FF(I,J) : temporary T_e
73-75 Computation of $\Delta T = T_{i,j} - T_{e,i,j}$

Subroutine SENSOR

Line

8-10 EMYL,ESILV,ESOLD : ϵ_M , ϵ_{ag} , ϵ_s
11-13 ALMYL,ALSILV,ALSOLD : α_M , α_{ag} , α_s
14-16 DMYL,DSILV,DSOL : thickness of Mylar, silver, solder,
 respectively
17-19 CMYL,CSILV,CSOLD : specific heat of Mylar, silver, solder,
 respectively

20-22 RCMYL,RCSILV,RC SOLD : ρ_c of Mylar, silver, solder,
 respectively
 24-35 Assignment of emissivity, k_d , ρ_{cd} to different regions
 36-79 COC(I,J) : $(k_d)_{i,j}$
 ROC(I,J) : $(\rho_{cd})_{i,j}$
 94-97 AKD(I,J),BKD(I,J),CKD(I,J),DKD(I,J) : $(AKD)_{i,j}$,
 $(BKD)_{i,j}$, $(CKD)_{i,j}$, $(DKD)_{i,j}$

ENVIRO

Line

4 Subroutine TREC is called to obtain T_r
 5 $H_l(I)$ is local convective coefficient $h(y)$
 7-14 $F(J,K) : f_{j,k}$
 $ALF(J,K,L) : \alpha_{j,k,\ell}$
 $BET(J) : \beta_j$
 $AI(J) : I_j$
 23-28 Radiation heat input for each film region

TREC

Line

4 AMFP,VEL,RHO,AMU,TINF : mean free path, velocity,
 density, viscosity, and $T_{(env)}$ of air at the altitude ALT.
 5 ALT : altitude
 7 X : distance from the leading edge
 8 AKNF : Knudsen number (referred to plate length)
 9 REF : Reynolds number

10 AKNFT : local Knudsen number (referred to boundary
layer thickness)
11 RFL : local recovery factor
12 TR : Tr

GANDF

Line

6 SIGM : Stefan-Boltzmann constant (σ)
21-22 QSENS,QSOND : heat flow from bead and sonde wires

COMP1

Line

24-35 Gauss' elimination process
34 U(I,J) : temporary temperature distribution

COMP2

Line

24-35 Gauss' elimination process
34 U(I,J) : temporary temperature distribution

GLOSSARY

A	area of a grid element
a,b	linearization coefficients of T^4 at T_a : $(-3T_a^4)$, $(4T_a^3)$.
c	specific heat of the plate
d	thickness of the plate
d_w	diameter of the wire
f, $f_{i,j}$	geometric factor
g	total convection coefficient
h	convection coefficient
h_1	convection coefficient, "front" side
h_2	convection coefficient, "back" side
h_x	local convection coefficient
I	radiant emittance
k	thermal conductivity, plate
k_w	thermal conductivity, wire
ℓ	length of the wire
q	heat input from a wire junction
q_r	heat input from radiation
q_{r1}	radiation input, front side
q_{r2}	radiation input, back side
r	recovery factor
r_x	local recovery factor
T_a	linearizing temperature
T_e	equilibrium temperature, without conduction

T_r	recovery temperature
$T_{(env)}$	atmospheric temperature
$T_{i,j}^p$	temperature of the plate at (i-j)th grid point at the pth time point
\dot{T}	derivative of temperature with respect to time
v	volume element
ΔX	grid size, lateral
ΔY	grid size, longitudinal
α	radiation absorptivity
α_{ag}	radiation absorptivity of silver
α_M	radiation absorptivity of Mylar
α_s	radiation absorptivity of solder
β	radiation perturbation factor
ϵ	radiation emissivity
ϵ_{ag}	silver radiation emissivity
ϵ_M	Mylar radiation emissivity
ϵ_s	solder radiation emissivity
ρ	mass density of plate
σ	Stefan-Boltzmann constant
τ	time constant

BIBLIOGRAPHY

- C. R. C. Handbook of Chemistry and Physics, 47th Edition, Cleveland, Ohio
The Chemical Rubber Company, 1966-1967.
- Drews, A. W., "Final Report on Research And Development to Improve
Temperature Measurement at High Altitudes," Report No. TR-PL-8876,
Atlantic Research Corporation, Report to National Aeronautics and
Space Administration, under contract NAS1-1611, January 1966.
- Dusinberre, G. M., Heat Transfer Calculations By Finite Differences,
International Textbook Company, Scranton, Pennsylvania, 1961.
- Forsythe, G. E. and W. R. Wasow, Finite Difference Methods for Partial
Differential Equations, John Wiley and Sons, Inc., New York, 1960.
- Peaceman, D. W. and H. H. Rachford, Jr., "The Numerical Solutions of
Parabolic and Elliptic Differential Equations," J. Sos. Indust.
Appl. Math., Vol. 3(1), March 1955.
- Staffanson, F. L., "Theoretical Comparison of Beads, Wires, and Films
as Rockets on Temperature Sensors in Mesosphere," Report No.
UTEC-MR-67-055, University of Utah, Progress Report to NASA,
under contract NGR 45-003-027.